EUROPEAN RESPIRATORY *journal*

FLAGSHIP SCIENTIFIC JOURNAL OF ERS

Early View

Original article

Crucial role for lung iron level and regulation in the pathogenesis and severity of asthma

Md Khadem Ali, Richard Y. Kim, Alexandra C. Brown, Jemma R. Mayall, Rafia Karim, James W. Pinkerton, Gang Liu, Kristy L. Martin, Malcolm R. Starkey, Amber Pillar, Chantal Donovan, Prabuddha S. Pathinayake, Olivia R. Carroll, Debbie Trinder, Hock L. Tay, Yusef E. Badi, Nazanin Z. Kermani, Yi-Ke Guo, Ritambhara Aryal, Sharon Mumby, Stelios Pavlidis, Ian M. Adcock, Jessica Weaver, Dikaia Xenaki, Brian G. Oliver, Elizabeth G. Holliday, Paul S. Foster, Peter A. Wark, Daniel M. Johnstone, Elizabeth A. Milward, Philip M. Hansbro, Jay C. Horvat

Please cite this article as: Ali MK, Kim RY, Brown AC, *et al*. Crucial role for lung iron level and regulation in the pathogenesis and severity of asthma. *Eur Respir J* 2020; in press (https://doi.org/10.1183/13993003.01340-2019).

ORIGINAL ARTICLE

Crucial role for lung iron level and regulation in the pathogenesis and severity of asthma

Md Khadem Ali[1,2], Richard Y. Kim[2,3], Alexandra C. Brown[2], Jemma R. Mayall[2], Rafia Karim[2], James W. Pinkerton[2,4], Gang Liu[2,3], Kristy L. Martin[5], Malcolm R. Starkey[2,6], Amber Pillar[2], Chantal Donovan[2,3], Prabuddha S. Pathinayake[7], Olivia R. Carroll[2], Debbie Trinder[8], Hock L. Tay[2], Yusef E. Badi[9], Nazanin Z. Kermani[10], Yi-Ke Guo[10], Ritambhara Aryal[5], Sharon Mumby[9], Stelios Pavlidis[9], Ian M. Adcock[9], Jessica Weaver[2], Dikaia Xenaki[11], Brian G. Oliver[11], Elizabeth G. Holliday[12], Paul S. Foster[2], Peter A. Wark[2,13], Daniel M. Johnstone[14], Elizabeth A. Milward[5], Philip M. Hansbro[2,3,#] and Jay C. Horvat[2#]

Affiliations: [1]Division of Pulmonary and Critical Care Medicine, Stanford University, California, United States of America. [2]Priority Research Centre for Healthy Lungs, Hunter Medical Research Institute and School of Biomedical Sciences and Pharmacy, University of Newcastle, Newcastle, New South Wales, Australia. [3]Centre for Inflammation, Centenary Institute, and Faculty of Science, University of Technology Sydney, Sydney, New South Wales, Australia. [4]Respiratory Pharmacology & Toxicology Group, National Heart & Lung Institute, Imperial College London, London, United Kingdom. [5]School of Biomedical Sciences and Pharmacy, The University of Newcastle, Newcastle, New South Wales, Australia. [6]Department of Immunology and Pathology, Central Clinical School, Monash

University, Melbourne, Victoria, Australia. [7]Priority Research Centre for Healthy Lungs, Hunter Medical Research Institute and School of Medicine and Public Health, University of Newcastle, Newcastle, New South Wales, Australia. [8]Medical School, Harry Perkins Medical Research Institute, University of Western Australia, Fiona Stanley Hospital, Perth, Western Australia, Australia. [9]Airway Disease Section, National Heart & Lung Institute, Imperial College London, London, United Kingdom. [10]Data science institute, Department of computing, Imperial College London. [11]Woolcock Institute of Medical Research, University of Sydney and School of Life Sciences, University of Technology Sydney, Sydney, NSW, Australia. [12]Hunter Medical Research Institute, New Lambton, New South Wales, Australia and School of Medicine and Public Health, University of Newcastle, Callaghan, New South Wales, Australia. [13]Department of Respiratory and Sleep Medicine, John Hunter Hospital, Newcastle, New South Wales, Australia. [14]Discipline of Physiology and Bosch Institute, University of Sydney, Sydney, New South Wales, Australia.

[#]Authors contributed equally

Correspondence to: Associate Professor Jay Horvat, PhD, School of Biomedical Sciences and Pharmacy, Faculty of Health and Medicine, The University of Newcastle, Callaghan, New South Wales, 2308, Australia, Tel: +61 2 4042 0220, F: +61 2 4042 0024, Email: jay.horvat@newcastle.edu.au

Take home message

The relationship between iron and the pathogenesis of asthma remains unclear. Here we show for the first time that altered iron responses are a key feature of clinical and experimental asthma and may play important roles in disease.

This article has supplementary material available from erj.ersjournals.com

Support statement: J.C.H. is supported by grants and fellowships from Cystic Fibrosis Australia and the Australian Cystic Fibrosis Research Trust and The University of Newcastle, Australia. P.M.H and D.T. are funded by Fellowships from the NHMRC (1079187 and 1020437). P.M.H. is also funded by an Investigator grant from the NHMRC of Australia (1175134).

Conflict of interest: Disclosures can be found alongside the online version of this article at erj.resjournals.com

Short Running Head: Iron and the pathogenesis and severity of asthma

ABSTRACT

Accumulating evidence highlights links between iron regulation and respiratory disease. Here, we assessed the relationship between iron levels and regulatory responses in clinical and experimental asthma.

We show that cell-free iron levels are reduced in the bronchoalveolar lavage (BAL) supernatant of severe or mild-moderate asthma patients and correlate with lower forced expiratory volume in one second (FEV1). Conversely, iron-loaded cell numbers were increased in BAL in these patients and with lower FEV1/forced vital capacity (FEV1/FVC). The airway tissue expression of the iron sequestration molecules divalent metal transporter 1 (*DMT1*) and transferrin receptor 1 (*TFR1)* are increased in asthma with *TFR1* expression correlating with reduced lung function and increased type 2 (T2) inflammatory responses in the airways. Furthermore, pulmonary iron levels are increased in a house dust mite (HDM)-induced model of experimental asthma in association with augmented *Tfr1* expression in airway tissue, similar to human disease. We show that macrophages are the predominant source of increased Tfr1 and $Tfr1^{+}$ macrophages have increased *Il13* expression. We also show that increased iron levels induce increased pro-inflammatory cytokine and/or extracellular matrix (ECM) responses in human airway smooth muscle (ASM) cells and fibroblasts *ex vivo* and induce key features of asthma, including airway hyper-responsiveness and fibrosis and T2 inflammatory responses, *in vivo*.

Together these complementary clinical and experimental data highlight the importance of altered pulmonary iron levels and regulation in asthma, and the need for a greater focus on the role and potential therapeutic targeting of iron in the pathogenesis and severity of disease.

Introduction

Clinical and experimental evidence suggests that altered levels of systemic and lung iron and/or iron regulatory molecules are associated with lung inflammation in many diseases including asthma (1). Chronic inflammatory responses that underpin many respiratory diseases are associated with decreased systemic iron levels (2, 3). There is a correlation between low maternal iron status during pregnancy with childhood wheezing, impaired lung function and atopic sensitisation (4), and low foetal iron is linked with increased susceptibility to eosinophilia in infancy (5). In a longitudinal study of parents and children, higher umbilical cord iron status was associated with decreased occurrence of wheezing and eczema, while lower iron status is linked to increased risk of atopy (6). Furthermore, lower serum and exhaled breath condensate iron levels are associated with asthma in children and adults (7-9). However, plasma iron and malondialdehyde levels, a marker of oxidative stress are significantly elevated in asthmatic subjects compared to healthy controls (10, 11). Ferritin levels are increased in the lungs in an experimental mouse model of asthma (12). Ferritin and iron levels were reduced by intranasal administration of iron chelator complexes in this model, with treatment also attenuating inflammation (12). By contrast, short-term intraperitoneal injection of iron dextran suppresses hallmark features of asthma in an acute mouse model (13), suggesting that increasing systemic iron levels may protect against disease. However, the potential pathological effects of chronically increasing systemic iron levels, and the effects on iron accumulation in the lung in asthma remain unexplored. Together, these findings provide evidence that asthma is associated with altered iron homeostasis. However, it is unclear whether altered iron levels play roles in pathogenesis or are a consequence of disease. Further clinical and experimental studies investigating the link between iron and asthma are required to better understand the mechanisms involved and address whether increased or decreased pulmonary iron levels are detrimental. In order to

address this, we assessed the levels of iron and iron-related gene expression in the airways of patients with severe or mild-moderate asthma and healthy controls. We show that altered iron metabolism in the airways is associated with asthma. Specifically, reduced extracellular iron levels, and increased cellular iron accumulation and airway *TFR1* expression are linked with disease severity, suggesting that iron sequestration/accumulation in cells/tissues may play roles in asthma pathogenesis. We also show that experimental asthma is associated with increased airway *Tfr1* expression that corresponds with increased pulmonary iron accumulation. These findings led us to hypothesise that increased iron accumulation in the lung plays a key role in driving the key features of asthma. We confirmed this by showing that increased lung iron levels in two murine models of iron overload result in the development of key asthma features similar to that observed in HDM-induced experimental disease.

Methods

Full details are provided in online supplementary material.

Study approvals

All experiments were conducted with approval of the Human/Animal Ethics Committees of the University of Newcastle, Australia and the local ethics committees of the Unbiased Biomarkers in Prediction of respiratory disease outcomes (U-BIOPRED) clinical centres.

Clinical analyses

Levels of iron were assessed in bronchoalveolar lavage (BAL) cells from 11 severe and 12 mild-moderate, asthma patients and 13 healthy controls using Perl's-DAB. In the same

cohorts, iron regulatory factors were assessed in airway biopsy tissues using qPCR. Colorimetric non-haem iron assay was used to measure non-haem iron content in BAL supernatants collected from a second set of severe and mild-moderate asthma patients and healthy controls (n=10 subjects/group). In both sets of donors, asthma severity was categorised based on FEV1% predicted and asthma severity symptoms/day/night (**Tables 1 and 2**). The transcriptomic profile of iron regulatory factors was analysed in bronchial brushings of 39 severe and 29 mild-moderate asthmatics and 40 healthy controls within the U-BIOPRED cohort (14).

Iron overloaded mice; experimental asthma model; iron quantification; airway inflammation; small airway fibrosis; lung function, flow cytometry analyses of different cell populations in murine lung tissue, human primary ASM and lung fibroblast cell culture, primary bronchial airway epithelial cells (pBECs) cultured at the air-liquid interface (ALI)

Haemochromatosis protein gene (*Hfe*)-deficient ($Hfe^{-/-}$) and wild-type (WT) mice on an AKR background (36 weeks old) (15), and WT BALB/c mice (8 week-old) fed a high iron diet (supplemented with 2% carbonyl iron, HID) for 8 weeks, were used to model iron overload. House dust mite (HDM)-induced experimental asthma was induced in $Hfe^{-/-}$ and WT BALB/c mice fed HID, normal (control chow, CC) or low iron diets (LID) (**Figure E1**). Iron quantification, airway inflammation, small airway fibrosis, lung function, pulmonary cell population characterisations, cytokines and ECM responses in human primary ASM cells and lung fibroblasts and iron related gene expression in pBECs were assessed as previously described (16-34) and as outlined in the online supplement.

Statistics

Comparisons between two groups were performed using a non-parametric Mann-Whitney test. Comparisons between multiple groups were performed using Kruskal-Wallis one-way analysis of variance (ANOVA) with uncorrected Dunn's post-hoc test. AHR data were analysed using two-way repeated measures ANOVA with Bonferroni post-hoc test. Correlation analyses were performed using Spearman rank correlation.

Results

Iron levels in BAL supernatant are reduced, but iron-positive cell numbers in BAL are increased, in asthma

We first assessed cell-free non-haem iron levels and iron-loaded cell numbers in BAL obtained from severe or mild-moderate asthma patients and healthy controls. Iron levels in BAL supernatant were reduced in combined severe and mild-moderate asthma patients compared to healthy controls, with the greatest decrease in severe disease (**Figure 1A and B**). Non-haem iron levels positively correlate with FEV1% predicted but not FEV1/FVC (**Figure 1C and D**). Non-haem iron levels negatively correlate with inhaled corticosteroid (ICS) used in asthmatics (**Figure 1E**). In contrast, severe and mild-moderate asthma patients have increased numbers of iron-positive cells in BAL compared to healthy controls (**Figure 1F-H**). Iron-positive BAL cell numbers negatively correlate with FEV1/FVC but not FEV1% predicted (**Figure 1I and J**). Together these novel findings show that decreased extracellular iron levels in the airway lumen, but increased iron in BAL cells, correlate with declines in lung function in asthma, suggesting a relationship between cellular sequestration/accumulation of iron and impaired lung function.

Key iron sequestration molecules divalent metal transporter 1 (*DMT1*) and transferrin receptor 1 (*TFR1*) levels are increased in the airways of asthma patients

We next assessed whether iron sequestration molecules *DMT1* and *TFR1* levels are increased in the airways of asthmatics. *DMT1*and *TFR1* mRNA expression are increased in the airways of asthma patients compared to healthy controls (**Figure 2A and D**). *DMT1* and *TFR1* expression negatively correlates with FEV1/FVC with similar correlations observed for FEV1% predicted (**Figure 2B, C, E and F**). We confirm that *TFR1* expression is increased in airways brushings from a separate cohort of asthma patients (**Figure 2G**). Importantly, TFR1 expression is strongly and positively associated with group 2 innate lymphoid cells (*ILC2*) (35), interleukin 4 *(IL4), IL5* and *IL13* expression (**Figure 2H-K**). Collectively, these data provide evidence that increased iron sequestration into airway tissues and/or cells due to increased *DMT1* and *TFR1* expression may play crucial roles in the pathogenesis and severity of asthma.

Expression of iron uptake, transport, storage, and regulatory factors is altered in the airways and pBECs of asthma patients

We next assessed whether the expression of other iron related genes is altered in the airways of asthma patients. Severe asthma patients have increased iron uptake molecules, transferrin receptor 2 (*TFR2),* zinc transporter (ZIP14), natural resistance-associated macrophage protein 1 (*NRAMP1)* (*p*=0.08*)* and iron storage molecules ferritin heavy chain (*FTH*) (*p*=0.06) expression compared to healthy controls (**Figure 3A-D**). The levels of *NRAMP1, FTH,* ferritin light chain (*FTL*) and iron regulatory protein 1 (*IRP1)* expression is significantly

higher in the airways of mild asthma patients compared to healthy controls (**Figure 3C-F**). Hepcidin (*HAMP)* expression is decreased in severe asthma airways compared to healthy controls (p=0.06) (**Figure 3G**). Interestingly, *FTL* is lower in severe compared to mild asthma patients (**Figure 3E**). There is no significant change in iron exporter ferroportin (FPN) expression in any of the groups (**Figure 3H**). Together these data show that factors associated with increased intracellular iron uptake and storage are largely increased in the airways of asthma patients, which may explain the decreases in extracellular iron levels in BAL supernatant and increased iron accumulation in cells/tissues.

To explore which cells are associated with altered iron in the airways, we next assessed expression of *DMT1, TFR1, TFR2, ZIP14, NRAMP1, FTH, FTL, IRP1, FPN* in pBECs obtained from asthmatic patients and healthy controls cultured at the ALI. Like with mRNA expression changes observed in airway tissue biopsy and bronchial brushings, we show that *TFR1* and *TFR2* expression is significantly increased in the pBECs of asthmatics (**Figure 3J and K**). There is no significant change in expression of any other factors (**Figure 3I, L-Q**).

Iron levels and Tfr1^{+} macrophages are increased in the lungs in HDM-induced experimental asthma, and increased iron induces pathological responses in ASM cells and lung fibroblasts

We next determined whether the levels of iron and regulatory factors are similarly altered in HDM-induced experimental asthma (**Figure E2**) and whether exogenous iron alters cytokines and ECM responses in primary human ASM cells and lung fibroblasts. We show that HDM-induced experimental asthma is also associated with the accumulation of non-haem iron in lung tissue (**Figure 4A**), with iron accumulation mostly in macrophages around the airways (**Figure 4B**). We find increased numbers of iron-positive cells in BAL (**Figure 4C**) and

increased expression of *Tfr1* in the airways (**Figure 4D**) and transferrin levels in BAL supernatant (**Figure 4E**). Together, our clinical and experimental data provide evidence for increased iron accumulation in lung tissues and cells in asthma that are either playing a role in, and/or are a consequence of, the pathogenesis of asthma. We next assessed the cellular source of increased *Tfr1* using flow cytometry. We show that the number of $Tfr1^+$ cells are increased in HDM-challenged mice and that these cells are predominantly alveolar and interstitial macrophages (**Figure 4F**). These data suggest that HDM-induced experimental asthma is characterised by an increase in macrophages that sequester iron. To determine whether these $Tfr1^+$ macrophage populations have a different phenotype, we measured expression of *Il10*, *Tgfb*, *Ifng* and *Il13* in $Tfr1^+$ and $Tfr1^-$ macrophages in HDM-induced experimental asthma and saline-challenged controls (**Figure 4G-J**). We show that $Tfr1^+$ macrophages from HDM-challenged mice have increased *Il10* and *Il13* expression compared to those from saline-challenged controls as well $Tfr1^-$ macrophages from both saline- or HDM-challenged groups (**Figure 4G and J**). This suggests that iron-sequestering, $Tfr1^+$ macrophages may play a pathologic role in asthma by promoting T2 inflammatory responses.

To further characterise the potential effects of increased extracellular iron levels in tissues, we also exposed human ASM cells and fibroblasts to increasing concentrations of ferric ammonium citrate (FAC). Increasing concentrations of FAC increase pro-inflammatory cytokine (IL-6 and Il-8) production and/or ECM gene (*TNC*) expression by these cells (**Figure 4K-P**).

Hfe$^{-/-}$ iron overload mice have increased iron levels in the lung associated with increased features of asthma

We next assessed the consequences of increased iron accumulation in lung tissues and cells on the pathogenesis and severity of key features of asthma using murine models of iron

overload. In the absence of HDM treatment, sham (PBS)-treated *Hfe*$^{-/-}$ mice, which overload iron systemically (e.g. in liver, **Figure 5A**), have significantly higher lung iron levels compared to sham-treated, WT controls (**Figure 5B**). Whilst HDM increases iron levels in the lungs of WT mice compared to sham-treated WT controls, it does not further enhance levels in *Hfe*$^{-/-}$ mice (**Figure 5B**). Increased iron in all groups is predominantly deposited in macrophages surrounding the airways and in the alveoli (**Figure 5C**).

We also demonstrate that increased iron accumulation observed in sham-treated *Hfe*$^{-/-}$ mice is associated with increases in leukocyte numbers in BAL and lung interleukin 13 (*Il13*) expression, which lead to small airway fibrosis and AHR compared to sham-treated WT controls (**Figure 5D, E, J-M**). Indeed, these features were similar to those observed in HDM-treated WT controls. HDM treatment in *Hfe*$^{-/-}$ mice increased the severity of all of the disease features compared to HDM-treated, WT controls (**Figure 5D, E, J-M)**. Together, these data demonstrate that pulmonary iron accumulation alone can drive key features of asthma, and that a combination of iron overload and HDM treatment may contribute to more severe features of experimental asthma.

Diet-induced iron accumulation also increases key features of asthma

To confirm our findings with *Hfe*$^{-/-}$ mice, we next assessed the effects of HID-induced iron overload on disease features. Similar to our findings in *Hfe*$^{-/-}$ mice, WT mice fed a HID, which overload iron systemically (**Figure 6A**), have increased pulmonary iron levels compared to mice fed CC (**Figure 6B**). Furthermore, like findings in *Hfe*$^{-/-}$ mice, diet-induced iron overload increases lung iron levels following HDM treatment with similar levels observed in HDM-treated mice on HID and CC diets (**Figure 6B**). Consistent with findings in *Hfe*$^{-/-}$ mice, iron accumulation in the lungs of HID fed mice is associated with airway fibrosis and AHR in the absence of HDM treatment (**Figure 6H-K**). HID-induced increases

the severity of HDM-induced experimental asthma, with small airways fibrosis and AHR increased in HID compared to CC fed HDM-treated mice (**Figure 6H-K**). There were some discrepancies observed between the effects *Hfe*$^{-/-}$ mice compared to HID fed mice. HID-fed mice did not exhibit increases in BAL leukocyte numbers, but did have elevated tissue eosinophil numbers in HDM-induced experimental asthma (**Figures 6C-E**). These data confirm that increased iron accumulation in the lung can drive the pathogenesis and increase the severity of key asthma features.

Interestingly, mice fed a LID, despite having reduced liver iron levels (**Figure 6A**), do not have reduced lung iron levels in the absence of HDM treatment (**Figure 6B**). However, LID fed mice do have reduced lung iron accumulation in HDM-induced experimental asthma (**Figure 6B**), which is associated with decreases in total leukocyte numbers in BAL and MSC numbers around the airways (**Figure 6C, F and G**). The decrease in lung iron levels has no effect on HDM-induced airway fibrosis or AHR (**Figure 6H-K**).

Together, these data show that the relationships between lung iron levels and the pathogenesis and severity of asthma is complex. Nevertheless, these data provide new evidence that increased iron accumulation in the lung plays key roles in driving the characteristic features of asthma.

Discussion

Clinically, both low (7, 8) and high (10, 11, 36) systemic iron has been reported in asthma. In most clinical studies, iron levels are assessed systemically in serum/plasma but not locally in the lung with only one study showing that low iron in exhaled breath condensate is associated with asthma (9). However, it is unclear whether altered iron levels play a role in pathogenesis, or if they are a consequence, of disease. To investigate the potential role of iron

level and/or regulation in the lung in the pathogenesis and severity of asthma, we first assessed iron levels in the BAL supernatant and cells of patients with mild-moderate and severe asthma compared to healthy controls. We show, for the first time, that non-haem iron levels in BAL supernatant are markedly lower in asthma patients compared with healthy controls. Significantly, when the asthma patients are separated into mild-moderate and severe groups, non-haem iron levels are further significantly reduced in patients with severe asthma. In contrast to the decreased iron levels in BAL supernatant, we show that the number of iron-loaded cells are increased in the BAL of patients with mild-moderate and severe asthma. Both the levels of extracellular iron in supernatant and iron-loaded cell numbers in BAL correlate with lung function, with higher extracellular iron levels associated with better, and higher iron-positive cells associated with worse, lung function. This is the first report showing correlations between airway iron homeostasis and key lung function parameters. Taken together, our data suggest that lower extracellular, and higher intracellular, iron in the airways is associated with asthma and is linked with disease severity.

Our clinical data, suggesting that asthma is associated with increased iron sequestration/accumulation into cells and/or tissues, is supported by our findings that *DMT1* and/or *TFR1* expression is significantly increased in the airways in clinical and experimental asthma and correlate with impairment of lung function. In the lung, iron is mostly imported into cells by TFR1 as well as DMT1 and natural resistance-associated macrophage protein 1 (NRAMP1) (1, 37-39). Thus, increased expression of *DMT1* and *TFR1* may contribute to the decreased extracellular, and increased intracellular, iron that we observe in BAL of asthma patients. These changes may be a consequence of chronic inflammatory responses that underpin disease. Inflammation is a well-known promoter of iron sequestration into cells, predominantly due to cytokine-mediated modification of hepcidin responses (40). A previous study showed that liver specific *Hepc*$^{-/-}$ mice had increased iron in the lung similar to Hepc

globally deficient mice, suggesting that systemic hepcidin plays a predominant role in regulating iron levels in the lung (41). However, studies are still required to determine whether hepcidin regulation occurs at a subtle level locally within the lung. IL-6 also enhances TFR1 responses and iron uptake in hepatocytes (42). TFR expression is upregulated in the lungs of rats exposed to lipopolysaccharide (43). We extend these findings by showing that *TFR1* expression is associated with increased T2 inflammatory gene (*IL4*, *IL5* and *IL13*) expression the in asthmatic airways. We also show that $Tfr1^{+}$ macrophages are increased in the lungs during HDM-induced experimental asthma and that these cells display a phenotype of increased *Il13* expression. We also show that exogenous iron increases pro-inflammatory cytokine and ECM responses in human ASM cells and/or lung fibroblasts. Together these data suggest that increased extracellular iron levels in lung tissue may drive disease through increasing pathological responses ASM cells and fibroblasts. Our data suggest that increased iron sequestration by $Tfr1^{+}$ macrophages, perhaps as a protective response to increased extracellular iron levels and/or innate pro-inflammatory responses in the asthmatic airway, may result in the induction of T2 inflammatory responses that play a key role in the pathogenesis of asthma.

Whilst our initial findings suggest strong links between the sequestration/accumulation of iron into cells/tissues and the pathogenesis and severity of asthma, they do not show whether changes in iron homeostasis that result in increased iron accumulation in cells is a driver or consequence of disease. To investigate the roles of pulmonary iron accumulation in disease, we employed a complementary suite of murine models of iron overload and chronic HDM-induced experimental asthma. We show that both genetic (*Hfe*$^{-/-}$ mice) and dietary (mice fed a HID) models of iron overload result in significant accumulation of iron in lung tissues. This iron accumulation is similar to that observed in HDM-induced experimental asthma. Furthermore, iron overload-induced

pulmonary iron accumulation results in the presentation of many of the key features of asthma, including airways inflammation, type 2 cytokine (IL-13) production, airway fibrosis and AHR. Together, these data provide strong evidence that increased tissue iron levels play a key functional role in the pathogenesis and increased severity of asthma.

To conclude, complementary clinical and experimental studies show a strong relationship between iron level and regulation and the pathogenesis and severity of asthma. We show, for the first time, that altered levels of iron and iron-related gene expression in the airways of patients with asthma is linked with lung function with evidence for increased iron accumulation into tissues being detrimental for disease. Using murine models, we show that increased lung iron accumulation drives the pathogenesis and severity of key features of asthma. Due to the small amounts of tissue available or lack of available RNA we were not able to measure iron levels in airway tissue biopsies, or iron regulatory gene expression in BAL cells. We also used bronchoscopy samples from two different cohorts. These are limitations of the current study. Nevertheless, our findings highlight the need for further studies to investigate the mechanisms that underpin the effects of iron dysregulation on the pathogenesis and severity of asthma and to explore and test novel iron-targeted therapies. Given the interactions that occur between microbes and iron and the role of infection in asthma, further studies are also required to explore the inter-relationship between microbiomes, iron levels/regulation, mucosal immunity and asthma.

Acknowledgements

Supported by grants and fellowships from Cystic Fibrosis Australia and the Australian Cystic Fibrosis Research Trust and The University of Newcastle, Australia. P.M.H and D.T. are

funded by Fellowships from the NHMRC (1079187 and 1020437). P.M.H. is also funded by an Investigator grant from the NHMRC of Australia (1175134).

References

1. Ali MK, Kim RY, Karim R, Mayall JR, Martin KL, Shahandeh A, Abbasian F, Starkey MR, Loustaud-Ratti V, Johnstone D, Milward EA, Hansbro PM, Horvat JC. Role of iron in the pathogenesis of respiratory disease. *Int J Biochem Cell Biol* 2017; 88: 181-195.
2. Kemna E, Pickkers P, Nemeth E, van der Hoeven H, Swinkels D. Time-course analysis of hepcidin, serum iron, and plasma cytokine levels in humans injected with LPS. *Blood* 2005; 106: 1864-1866.
3. Cherayil BJ. Pathophysiology of Iron Homeostasis during Inflammatory States. *J Pediatr* 2015; 167: S15-19.
4. Nwaru BI, Hayes H, Gambling L, Craig LC, Allan K, Prabhu N, Turner SW, McNeill G, Erkkola M, Seaton A, McArdle HJ, Devereux G. An exploratory study of the associations between maternal iron status in pregnancy and childhood wheeze and atopy. *Br J Nutr* 2014; 112: 2018-2027.
5. Weigert R, Dosch NC, Bacsik-Campbell ME, Guilbert TW, Coe CL, Kling PJ. Maternal pregnancy weight gain and cord blood iron status are associated with eosinophilia in infancy. *J Perinatol* 2015; 35: 621-626.
6. Shaheen SO, Newson RB, Henderson AJ, Emmett PM, Sherriff A, Cooke M, Team AS. Umbilical cord trace elements and minerals and risk of early childhood wheezing and eczema. *Eur Respir J* 2004; 24: 292-297.

7. Ramakrishnan K, Borade A. Anemia as a risk factor for childhood asthma. *Lung India* 2010; 27: 51-53.

8. Brigham EP, McCormack MC, Takemoto CM, Matsui EC. Iron status is associated with asthma and lung function in US women. *PLoS One* 2015; 10: e0117545.

9. Vlasic Z, Dodig S, Cepelak I, Topic RZ, Zivcic J, Nogalo B, Turkalj M. Iron and ferritin concentrations in exhaled breath condensate of children with asthma. *J Asthma* 2009; 46: 81-85.

10. Kocyigit A, Armutcu F, Gurel A, Ermis B. Alterations in plasma essential trace elements selenium, manganese, zinc, copper, and iron concentrations and the possible role of these elements on oxidative status in patients with childhood asthma. *Biol Trace Elem Res* 2004; 97: 31-41.

11. Narula MK, Ahuja GK, Whig J, Narang AP, Soni RK. Status of lipid peroxidation and plasma iron level in bronchial asthmatic patients. *Indian J Physiol Pharmacol* 2007; 51: 289-292.

12. Bibi H, Vinokur V, Waisman D, Elenberg Y, Landesberg A, Faingersh A, Yadid M, Brod V, Pesin J, Berenshtein E, Eliashar R, Chevion M. Zn/Ga-DFO iron-chelating complex attenuates the inflammatory process in a mouse model of asthma. *Redox Biol* 2014; 2: 814-819.

13. Maazi H, Shirinbak S, Bloksma N, Nawijn MC, van Oosterhout AJ. Iron administration reduces airway hyperreactivity and eosinophilia in a mouse model of allergic asthma. *Clin Exp Immunol* 2011; 166: 80-86.

14. Kuo CS, Pavlidis S, Loza M, Baribaud F, Rowe A, Pandis I, Hoda U, Rossios C, Sousa A, Wilson SJ, Howarth P, Dahlen B, Dahlen SE, Chanez P, Shaw D, Krug N, Sandstrm T, De Meulder B, Lefaudeux D, Fowler S, Fleming L, Corfield J, Auffray C, Sterk PJ, Djukanovic R, Guo Y, Adcock IM, Chung KF, dagger UBPTd. A

Transcriptome-driven Analysis of Epithelial Brushings and Bronchial Biopsies to Define Asthma Phenotypes in U-BIOPRED. *Am J Respir Crit Care Med* 2017; 195: 443-455.

15. Zhou XY, Tomatsu S, Fleming RE, Parkkila S, Waheed A, Jiang J, Fei Y, Brunt EM, Ruddy DA, Prass CE, Schatzman RC, O'Neill R, Britton RS, Bacon BR, Sly WS. HFE gene knockout produces mouse model of hereditary hemochromatosis. *Proc Natl Acad Sci U S A* 1998; 95: 2492-2497.
16. Gold MJ, Hiebert PR, Park HY, Stefanowicz D, Le A, Starkey MR, Deane A, Brown AC, Liu G, Horvat JC, Ibrahim ZA, Sukkar MB, Hansbro PM, Carlsten C, VanEeden S, Sin DD, McNagny KM, Knight DA, Hirota JA. Mucosal production of uric acid by airway epithelial cells contributes to particulate matter-induced allergic sensitization. *Mucosal Immunol* 2016; 9: 809-820.
17. Kaldor I. Studies on intermediary iron metabolism. V. The measurement of non-haemoglobin tissue iron. *Aust J Exp Biol Med Sci* 1954; 32: 795-799.
18. Collison A, Hatchwell L, Verrills N, Wark PA, de Siqueira AP, Tooze M, Carpenter H, Don AS, Morris JC, Zimmermann N, Bartlett NW, Rothenberg ME, Johnston SL, Foster PS, Mattes J. The E3 ubiquitin ligase midline 1 promotes allergen and rhinovirus-induced asthma by inhibiting protein phosphatase 2A activity. *Nat Med* 2013; 19: 232-237.
19. Horvat JC, Starkey MR, Kim RY, Phipps S, Gibson PG, Beagley KW, Foster PS, Hansbro PM. Early-life chlamydial lung infection enhances allergic airways disease through age-dependent differences in immunopathology. *J Allergy Clin Immunol* 2010; 125: 617-625, 625 e611-625 e616.

20. Asquith KL, Horvat JC, Kaiko GE, Carey AJ, Beagley KW, Hansbro PM, Foster PS. Interleukin-13 promotes susceptibility to chlamydial infection of the respiratory and genital tracts. *PLoS Pathog* 2011; 7: e1001339.

21. Beckett EL, Stevens RL, Jarnicki AG, Kim RY, Hanish I, Hansbro NG, Deane A, Keely S, Horvat JC, Yang M, Oliver BG, van Rooijen N, Inman MD, Adachi R, Soberman RJ, Hamadi S, Wark PA, Foster PS, Hansbro PM. A new short-term mouse model of chronic obstructive pulmonary disease identifies a role for mast cell tryptase in pathogenesis. *J Allergy Clin Immunol* 2013; 131: 752-762.

22. Liu G, Cooley MA, Jarnicki AG, Hsu AC, Nair PM, Haw TJ, Fricker M, Gellatly SL, Kim RY, Inman MD, Tjin G, Wark PA, Walker MM, Horvat JC, Oliver BG, Argraves WS, Knight DA, Burgess JK, Hansbro PM. Fibulin-1 regulates the pathogenesis of tissue remodeling in respiratory diseases. *JCI Insight* 2016; 1.

23. Horvat JC, Starkey MR, Kim RY, Beagley KW, Preston JA, Gibson PG, Foster PS, Hansbro PM. Chlamydial respiratory infection during allergen sensitization drives neutrophilic allergic airways disease. *J Immunol* 2010; 184: 4159-4169.

24. Kim RY, Horvat JC, Pinkerton JW, Starkey MR, Essilfie AT, Mayall JR, Nair PM, Hansbro NG, Jones B, Haw TJ, Sunkara KP, Nguyen TH, Jarnicki AG, Keely S, Mattes J, Adcock IM, Foster PS, Hansbro PM. MicroRNA-21 drives severe, steroid-insensitive experimental asthma by amplifying phosphoinositide 3-kinase-mediated suppression of histone deacetylase 2. *J Allergy Clin Immunol* 2017; 139: 519-532.

25. Nair PM, Starkey MR, Haw TJ, Liu G, Horvat JC, Morris JC, Verrills NM, Clark AR, Ammit AJ, Hansbro PM. Targeting PP2A and proteasome activity ameliorates features of allergic airway disease in mice. *Allergy* 2017; 72: 1891-1903.

26. Liu G, Cooley MA, Nair PM, Donovan C, Hsu AC, Jarnicki AG, Haw TJ, Hansbro NG, Ge Q, Brown AC, Tay H, Foster PS, Wark PA, Horvat JC, Bourke JE, Grainge CL,

Argraves WS, Oliver BG, Knight DA, Burgess JK, Hansbro PM. Airway remodelling and inflammation in asthma are dependent on the extracellular matrix protein fibulin-1c. *J Pathol* 2017; 243: 510-523.

27. Essilfie AT, Horvat JC, Kim RY, Mayall JR, Pinkerton JW, Beckett EL, Starkey MR, Simpson JL, Foster PS, Gibson PG, Hansbro PM. Macrolide therapy suppresses key features of experimental steroid-sensitive and steroid-insensitive asthma. *Thorax* 2015; 70: 458-467.
28. Thorburn AN, Foster PS, Gibson PG, Hansbro PM. Components of Streptococcus pneumoniae suppress allergic airways disease and NKT cells by inducing regulatory T cells. *J Immunol* 2012; 188: 4611-4620.
29. Hansbro PM, Hamilton MJ, Fricker M, Gellatly SL, Jarnicki AG, Zheng D, Frei SM, Wong GW, Hamadi S, Zhou S, Foster PS, Krilis SA, Stevens RL. Importance of mast cell Prss31/transmembrane tryptase/tryptase-gamma in lung function and experimental chronic obstructive pulmonary disease and colitis. *J Biol Chem* 2014; 289: 18214-18227.
30. Kaiko GE, Phipps S, Hickey DK, Lam CE, Hansbro PM, Foster PS, Beagley KW. Chlamydia muridarum infection subverts dendritic cell function to promote Th2 immunity and airways hyperreactivity. *J Immunol* 2008; 180: 2225-2232.
31. Thorburn AN, O'Sullivan BJ, Thomas R, Kumar RK, Foster PS, Gibson PG, Hansbro PM. Pneumococcal conjugate vaccine-induced regulatory T cells suppress the development of allergic airways disease. *Thorax* 2010; 65: 1053-1060.
32. Krimmer D, Ichimaru Y, Burgess J, Black J, Oliver B. Exposure to biomass smoke extract enhances fibronectin release from fibroblasts. *PLoS One* 2013; 8: e83938.
33. Hsu AC, Starkey MR, Hanish I, Parsons K, Haw TJ, Howland LJ, Barr I, Mahony JB, Foster PS, Knight DA, Wark PA, Hansbro PM. Targeting PI3K-p110alpha

Suppresses Influenza Virus Infection in Chronic Obstructive Pulmonary Disease. *Am J Respir Crit Care Med* 2015; 191: 1012-1023.

34. Starkey MR, Nguyen DH, Brown AC, Essilfie AT, Kim RY, Yagita H, Horvat JC, Hansbro PM. Programmed Death Ligand 1 Promotes Early-Life Chlamydia Respiratory Infection-Induced Severe Allergic Airway Disease. *Am J Respir Cell Mol Biol* 2016; 54: 493-503.
35. Bjorklund AK, Forkel M, Picelli S, Konya V, Theorell J, Friberg D, Sandberg R, Mjosberg J. The heterogeneity of human CD127(+) innate lymphoid cells revealed by single-cell RNA sequencing. *Nat Immunol* 2016; 17: 451-460.
36. Ekmekci OB, Donma O, Sardogan E, Yildirim N, Uysal O, Demirel H, Demir T. Iron, nitric oxide, and myeloperoxidase in asthmatic patients. *Biochemistry (Mosc)* 2004; 69: 462-467.
37. Cloonan SM, Mumby S, Adcock IM, Choi AMK, Chung KF, Quinlan GJ. The IRONy of Iron-overload and Iron-deficiency in Chronic Obstructive Pulmonary Disease. *Am J Respir Crit Care Med* 2017.
38. Kim J, Molina RM, Donaghey TC, Buckett PD, Brain JD, Wessling-Resnick M. Influence of DMT1 and iron status on inflammatory responses in the lung. *Am J Physiol Lung Cell Mol Physiol* 2011; 300: L659-665.
39. Ghio AJ, Carter JD, Richards JH, Richer LD, Grissom CK, Elstad MR. Iron and iron-related proteins in the lower respiratory tract of patients with acute respiratory distress syndrome. *Crit Care Med* 2003; 31: 395-400.
40. Ganz T, Nemeth E. Iron homeostasis in host defence and inflammation. *Nat Rev Immunol* 2015; 15: 500-510.
41. Deschemin JC, Mathieu JRR, Zumerle S, Peyssonnaux C, Vaulont S. Pulmonary Iron Homeostasis in Hepcidin Knockout Mice. *Front Physiol* 2017; 8: 804.

42. Ahmad S, Sultan S, Naz N, Ahmad G, Alwahsh SM, Cameron S, Moriconi F, Ramadori G, Malik IA. Regulation of iron uptake in primary culture rat hepatocytes: the role of acute-phase cytokines. *Shock* 2014; 41: 337-345.

43. Upton RL, Chen Y, Mumby S, Gutteridge JM, Anning PB, Nicholson AG, Evans TW, Quinlan GJ. Variable tissue expression of transferrin receptors: relevance to acute respiratory distress syndrome. *Eur Respir J* 2003; 22: 335-341.

Figure legends

Figure 1. Iron regulation in the airways is altered in asthma. Non-haem iron (NHI) levels were measured in bronchoalveolar lavage (BAL) supernatant collected from patients with severe or mild-moderate asthma and healthy controls (n=10/group) (A, B). Non-haem iron levels were correlated with FEV1% predicted and FEV1/FVC (C, D). Non-haem iron levels were negatively correlated with inhaled corticosteroid (ICS) use (E). BAL cells were stained with Perl's-DAB and iron-positive cells enumerated (n=8-10) (F-H). Correlations between iron-positive cells and FEV1% predicted, and FEV1/FVC (I, J). Correlations for each comparison are represented as Spearman rank correlation coefficient (Spearman rho; r). Data are presented as means ± SEM. *p<0.05, **p<0.01 compared to respective controls.

Figure 2. Increased *DMT1* and *TFR1* expression in the airways correlates with impaired lung function in asthma patients. *DMT1* and *TFR1* mRNA expression was quantified in the airway tissues collected from 7 severe and 7 mild-moderate asthmatic patients, and 6 healthy controls using qPCR (A, D). Relative expression to the reference gene beta (β)-*actin* was performed. *DMT1* and *TFR1* expression levels negatively correlate with FEV1% predicted and FEV1/FVC (B, C and E, F). Correlations for each comparison are represented as

Spearman rank correlation coefficient (Spearman rho; *r*). *TFR1* mRNA expression in the bronchial brushings of asthma patients within U-BIOPRED cohort (G). TFR1 expression was positively correlated with *ILC2*, *IL4*, *IL5* and *IL13* expression (H-K)**.** Data are presented as means ± SEM. *$p<0.05$, **$p<0.01$ compared to respective controls.

Figure 3. Altered expressions of iron regulatory factors in the airways of asthma patients. The mRNA expression of *TFR2* (A), *ZIP14* (B), *NRAMP1* (C), *FTH* (D), *FTL* (E), *IRP1* (F), *HAMP* (G) and *FPN* (H) was assessed in the airway tissues collected from 7 severe and 7 mild-moderate asthma patients and 6 healthy controls using qPCR. The mRNA expression of *DMT1* (I), *TFR1(J), TFR2* (K), *ZIP14* (L), *NRAMP1* (M), *FTH* (N), *FTL* (O), *IRP1* (P) and *FPN* (Q) was also assessed using qPCR in primary bronchial epithelial cells obtained from 7 severe asthmatic patients and 8 healthy controls that have been cultured at the air-liquid interface (ALI). Relative expression to the reference gene *β-actin and GAPDH* is presented. Relative expression to the reference gene *β-actin* is presented. Data are presented as means ± SEM. *$p<0.05$, **$p<0.01$ compared to respective controls.

Figure 4. Iron levels are increased in the lung in house dust mite (HDM)-induced experimental asthma. Six-8 week old wild-type (WT) BALB/c mice were intranasally administered HDM antigen for 5 days per week for 6 weeks and then major features of HDM-induced experimental asthma were assessed. Non-haem iron (NHI) content was measured in the lung homogenates (A). Localisation of iron in the lung was assessed in Perls'-DAB stained lung sections (B). Iron-positive cells were enumerated in Perls-stained BAL cells (C). *Tfr1* expression was measured in the airways tissue using qPCR (D). Transferrin levels were measured by ELISA (E). $Tfr1^+$ cells were sorted using FACS analysis (F). Expression of Il10, Tgfb, Ifng and Il13 was assessed in sorted $Tfr1^+$ and $Tfr1^-$

macrophages in the presence and absence of HDM-induced experimental asthma using qPCR (G-J). Levels of *TNC* and IL6 and IL8 were measured in FAC-treated ASM and lung fibroblast cells using qPCR and ELISA, respectively (K-P). Scale bar: 50 μm. Data are presented as mean ± SEM (*n*=6-8), pooled from two repeat experiments. ***p*<0.01; ****p*<0.001; *****p*<0.0001 compared to PBS controls.

Figure 5. Absence of *Hfe* increases the severity of house dust mite (HDM)-induced experimental asthma. HDM was administered to ~36 weeks old wild-type (WT) AKR and *Hfe*$^{-/-}$ mice for 5 days per week for 6 weeks and then the hallmark features of experimental asthma were assessed. (A) Levels of non-haem iron (NHI) were measured in the liver (A) and lung (B). Localisation of iron in the lung was assessed in Perls'-DAB stained lung sections (C). Total leukocytes were enumerated in processed BAL (D). *Il13* mRNA expression was measured by qPCR (E). Tissue eosinophilic inflammation was quantified in chrome salt fixation-stained lung sections (F, G). Mucus secreting cells were enumerated around the airways in PAS-stained lung sections (H, I). Area of collagen deposition surrounding the basement membrane of small airways was determined in Sirius red-stained lung tissue sections, in 6-8 airways/mouse using *ImageJ* (J, K). Airways hyper-responsiveness (AHR), in terms of central airway resistance (Rn), was measured in response to increasing concentrations of nebulised methacholine (Mch) (L). Rn at 10mg/mL Mch was determined from AHR curves (M). Scale bar: 50 μm. Data are presented as mean ± SEM (*n*=6-10), pooled from two repeat experiments. **p*<0.05; ***p*<0.01; ****p*<0.001; *****p*<0.0001.

Figure 6. High iron diet-induced iron accumulation increases the key features of asthma. Wild-type (WT) BALB/c female mice (6-8 weeks old) were fed low iron (LID), normal control chow (CC) and high iron diets (HID) and were intranasally administered

house dust mite (HDM) antigen or PBS 5 days a week for up to 6 weeks. Non-haem iron (NHI) content was measured in the liver and lung by non-haem iron assay (A, B). Total leukocytes were enumerated in the processed BAL (C). Numbers of eosinophils were quantified around the most inflamed airways in chrome salt fixation-stained lung sections (D, E). Mucus secreting cells were enumerated around airways in PAS-stained lung sections (F, G). Area of collagen deposition surrounding the basement membrane of small airways was quantified in Sirius red-stained lung tissue sections, in 6-8 airways/mouse using *ImageJ* (H, I). Airways hyper-responsiveness (AHR) in terms of central airway resistance (Rn) was measured in response to inhaled increasing concentrations of methacholine (Mch) (J). Rn at 30mg/mL Mch was determined from AHR curves (K). Scale bar: 50 μm. Data are presented as mean ± SEM (n=6-19), pooled from 3 repeat experiments. *p<0.05; **p<0.01; ***p<0.001; ****p<0.0001 compared to respective controls.

Table 1. Human sample donor characteristics (Iron metabolism genes expression in airway biopsy tissues and iron scores in BAL cells)

Table 2. Human sample donor characteristics (Non-heme iron quantification in BAL)

Figure 1.

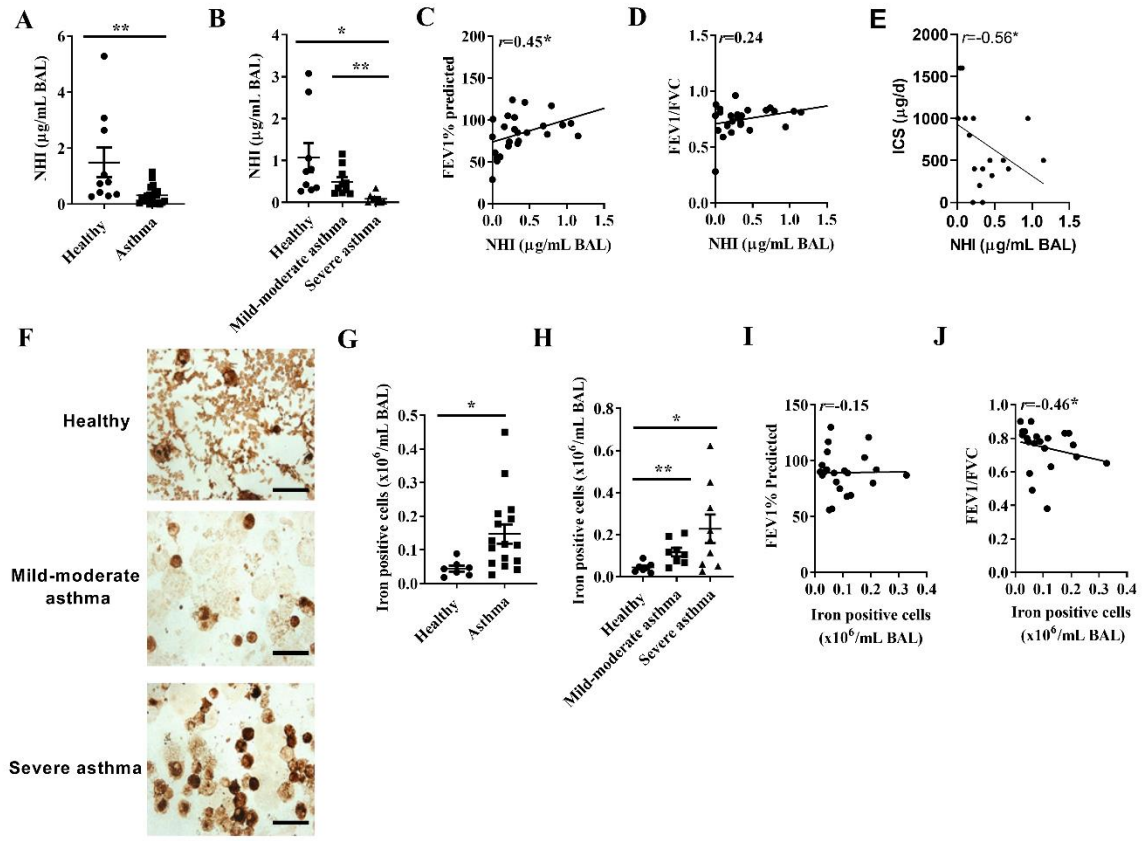
A
B
C
D
E
NHI (µg/mL BAL)
Healthy
Asthma
Mild-moderate asthma
Severe asthma
FEV1% predicted
r=0.45*
FEV1/FVC
r=0.24
ICS (µg/d)
r=-0.56*
F
G
H
I
J
Iron positive cells (x10^6/mL BAL)
r=-0.15
FEV1% Predicted
r=-0.46*

Figure 2.

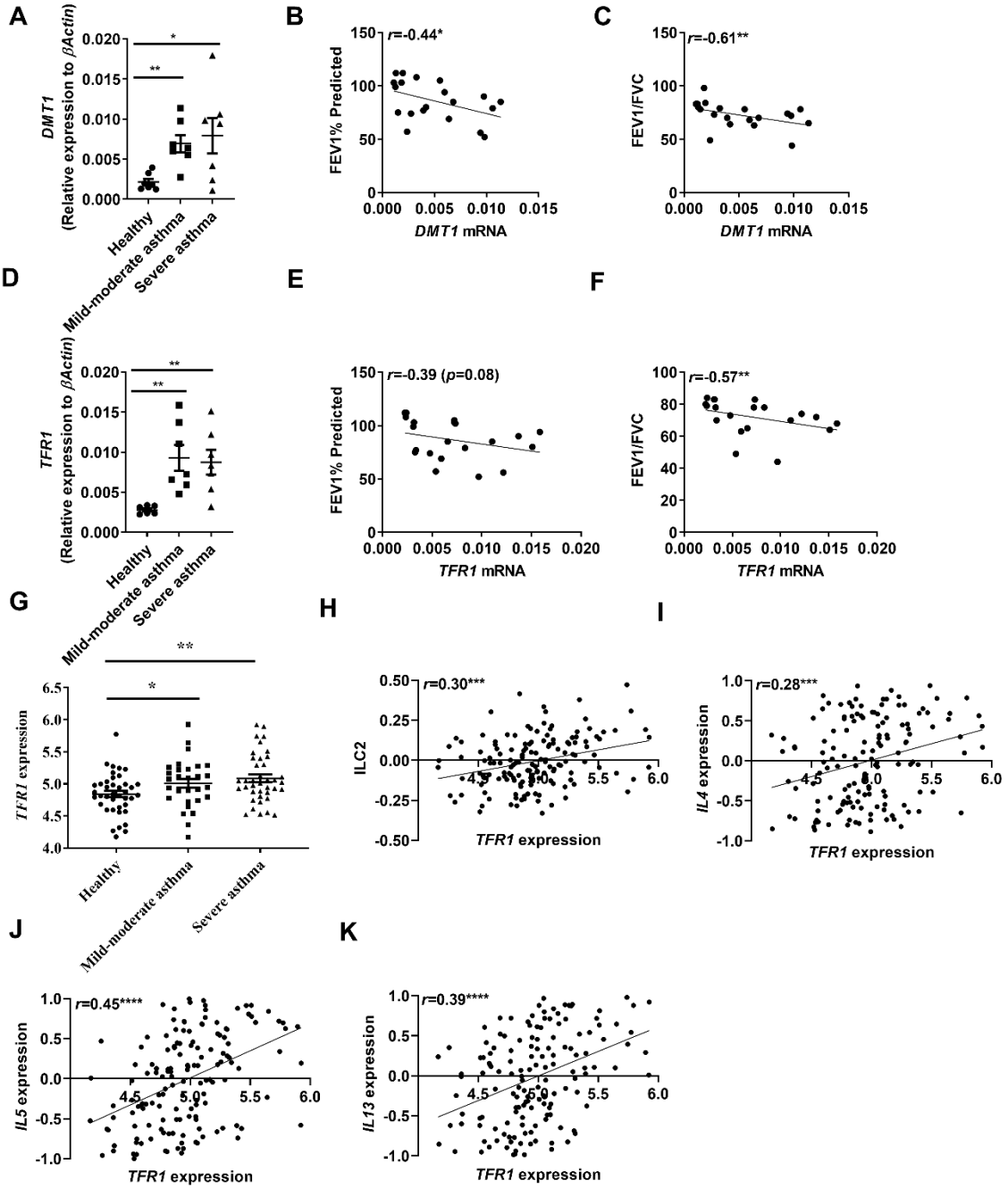
A
DMT1 (Relative expression to βActin)
0.020
0.015
0.010
0.005
0.000
*
**
Healthy
Mild-moderate asthma
Severe asthma
B
r=-0.44*
FEV1% Predicted
150
100
50
0
0.000 0.005 0.010 0.015
DMT1 mRNA
C
r=-0.61**
FEV1/FVC
150
100
50
0
0.000 0.005 0.010 0.015
DMT1 mRNA
D
TFR1 (Relative expression to βActin)
0.020
0.015
0.010
0.005
0.000
**
**
Healthy
Mild-moderate asthma
Severe asthma
E
r=-0.39 (p=0.08)
FEV1% Predicted
150
100
50
0
0.000 0.005 0.010 0.015 0.020
TFR1 mRNA
F
r=-0.57**
FEV1/FVC
100
80
60
40
20
0
0.000 0.005 0.010 0.015 0.020
TFR1 mRNA
G
**
*
TFR1 expression
6.5
6.0
5.5
5.0
4.5
4.0
Healthy
Mild-moderate asthma
Severe asthma
H
r=0.30***
ILC2
0.50
0.25
0.00
-0.25
-0.50
4.5 5.0 5.5 6.0
TFR1 expression
I
r=0.28***
IL4 expression
1.0
0.5
0.0
-0.5
-1.0
4.5 5.0 5.5 6.0
TFR1 expression
J
r=0.45****
IL5 expression
1.0
0.5
0.0
-0.5
-1.0
4.5 5.0 5.5 6.0
TFR1 expression
K
r=0.39****
IL13 expression
1.0
0.5
0.0
-0.5
-1.0
4.5 5.0 5.5 6.0
TFR1 expression

Figure 3.

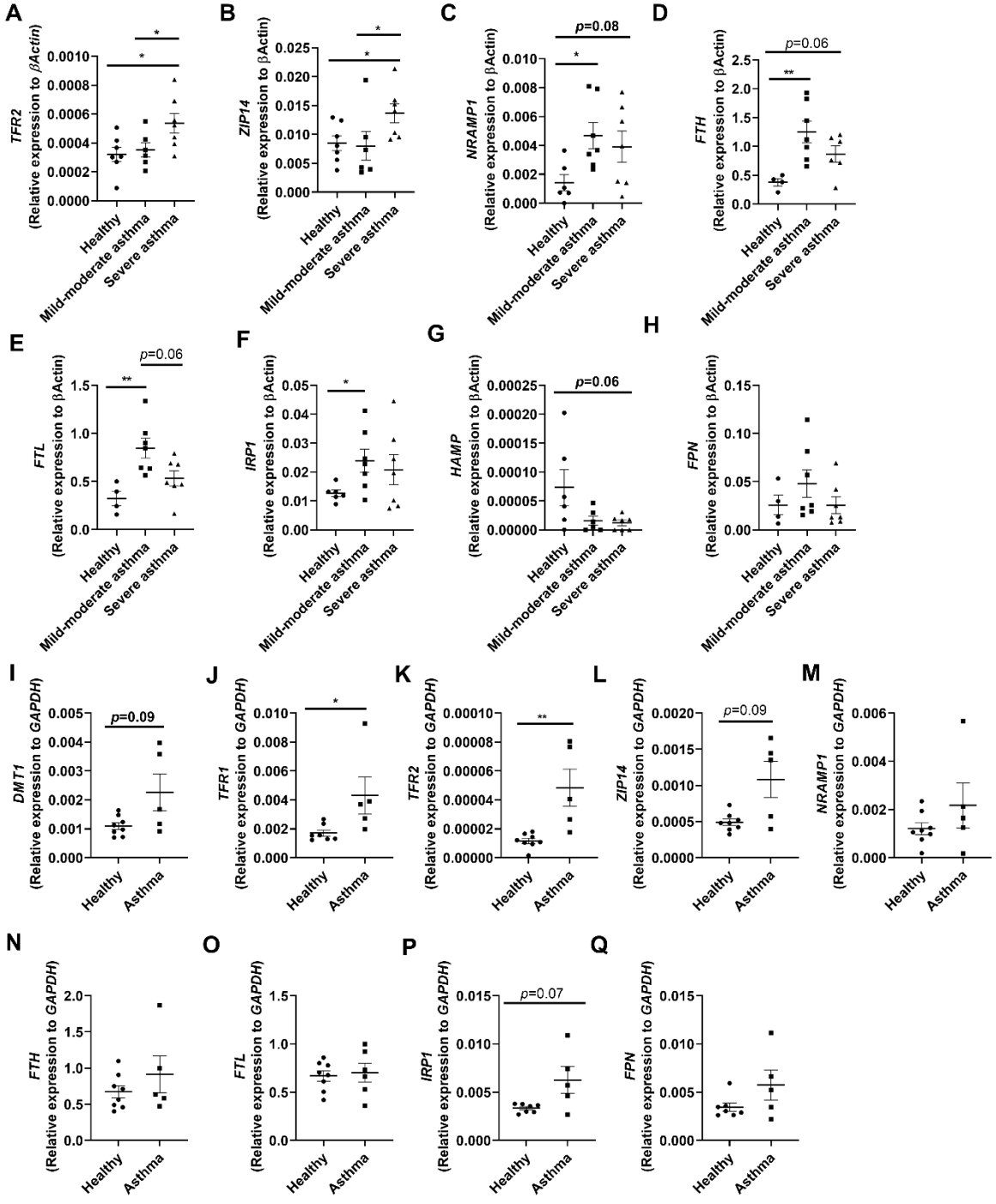
A
TFR2
(Relative expression to βActin)
B
ZIP14
(Relative expression to βActin)
C
NRAMP1
(Relative expression to βActin)
p=0.08
D
FTH
(Relative expression to βActin)
p=0.06
E
FTL
(Relative expression to βActin)
p=0.06
F
IRP1
(Relative expression to βActin)
G
HAMP
(Relative expression to βActin)
p=0.06
H
FPN
(Relative expression to βActin)
Healthy
Mild-moderate asthma
Severe asthma
I
DMT1
(Relative expression to GAPDH)
p=0.09
J
TFR1
(Relative expression to GAPDH)
K
TFR2
(Relative expression to GAPDH)
L
ZIP14
(Relative expression to GAPDH)
p=0.09
M
NRAMP1
(Relative expression to GAPDH)
N
FTH
(Relative expression to GAPDH)
O
FTL
(Relative expression to GAPDH)
P
IRP1
(Relative expression to GAPDH)
p=0.07
Q
FPN
(Relative expression to GAPDH)
Healthy
Asthma

Figure 4.

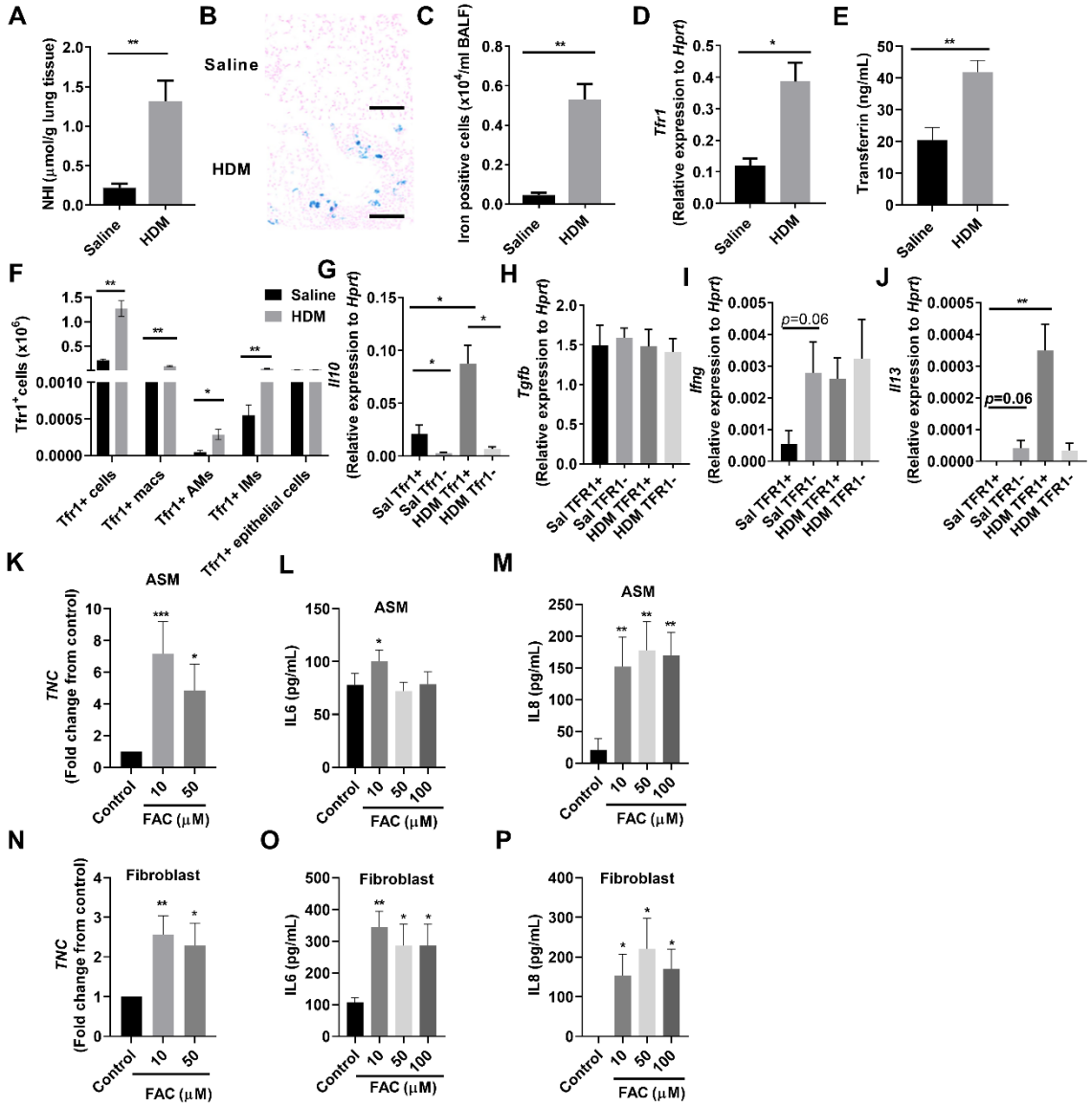
A
NHI (μmol/g lung tissue)
Saline
HDM
B
Saline
HDM
C
Iron positive cells (x10⁴/ml BALF)
D
Tfr1 (Relative expression to Hprt)
E
Transferrin (ng/mL)
F
Tfr1⁺cells (x10⁶)
Saline
HDM
Tfr1+ cells
Tfr1+ macs
Tfr1+ AMs
Tfr1+ IMs
Tfr1+ epithelial cells
G
Il10 (Relative expression to Hprt)
Sal Tfr1+
Sal Tfr1-
HDM Tfr1+
HDM Tfr1-
H
Tgfb (Relative expression to Hprt)
Sal TFR1+
Sal TFR1-
HDM TFR1+
HDM TFR1-
I
Ifng (Relative expression to Hprt)
p=0.06
J
Il13 (Relative expression to Hprt)
p=0.06
K
ASM
TNC (Fold change from control)
Control
FAC (μM)
L
ASM
IL6 (pg/mL)
M
ASM
IL8 (pg/mL)
N
Fibroblast
TNC (Fold change from control)
O
Fibroblast
IL6 (pg/mL)
P
Fibroblast
IL8 (pg/mL)

Figure 5.

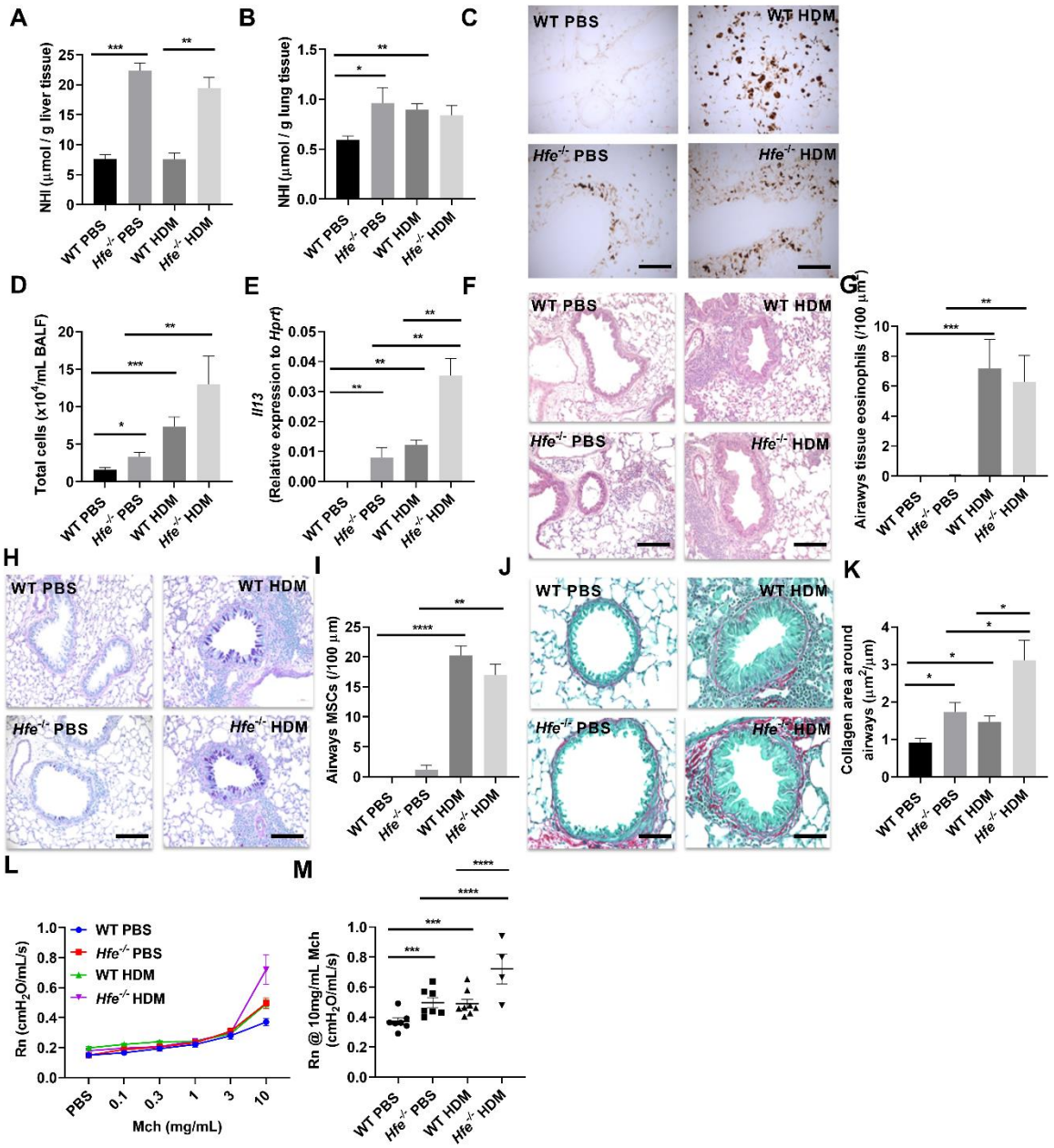
A
NHI (µmol / g liver tissue)
WT PBS
Hfe-/- PBS
WT HDM
Hfe-/- HDM
B
NHI (µmol / g lung tissue)
C
WT PBS
WT HDM
Hfe-/- PBS
Hfe-/- HDM
D
Total cells (x10⁴/mL BALF)
E
Il13
(Relative expression to Hprt)
F
G
Airways tissue eosinophils (/100 µm²)
H
I
Airways MSCs (/100 µm)
J
K
Collagen area around airways (µm²/µm)
L
Rn (cmH2O/mL/s)
PBS
0.1
0.3
1
3
10
Mch (mg/mL)
M
Rn @ 10mg/mL Mch (cmH2O/mL/s)

Figure 6.

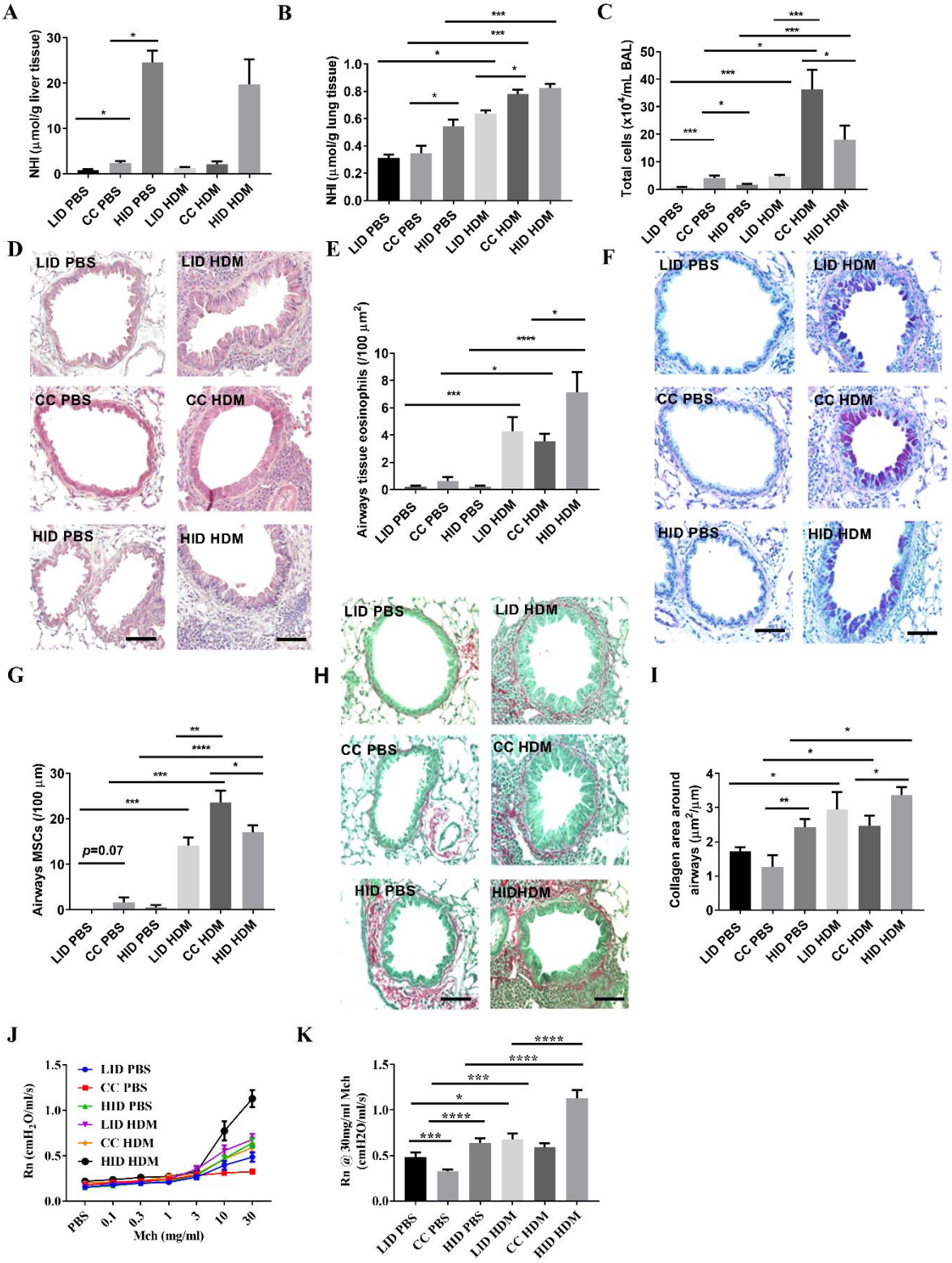
A
NHI (µmol/g liver tissue)
LID PBS
CC PBS
HID PBS
LID HDM
CC HDM
HID HDM
B
NHI (µmol/g lung tissue)
C
Total cells (x10⁴/mL BAL)
D
E
Airways tissue eosinophils (/100 µm²)
F
G
Airways MSCs (/100 µm)
p=0.07
H
HIDHDM
I
Collagen area around airways (µm²/µm)
J
Rn (cmH₂O/ml/s)
Mch (mg/ml)
PBS
0.1
0.3
1
3
10
30
K
Rn @ 30mg/ml Mch (cmH2O/ml/s)

Table 1.

Characteristic	Healthy	Mild-moderate asthmatics	Severe asthmatics
Number of subjects, n	13	12	11
Age, yr	53.00 ± 4.729	55.92 ± 4.583	53.73 ± 3.681
Sex, M/F	4/9	6/6	2/9
BMI (kg/m^2)	-	31.22 ± 2.302	31.71 ± 4.313
FEV1% predicted	102.7 ± 4.494	86.92 ± 2.726**	76 ± 5.389***
FEV1/FVC	0.817 ± 0.021	0.730 ± 0.016**	0.656 ± 0.049**
ACQ	-	0.903 ± 0.168	2.166 ± 0.291$^{\#\#}$
Total cells (x10^6/mL BAL)	0.170 ± 0.026	0.129 ± 0.021	0.853 ± 0.327$^{*, \#}$
Macrophages (x10^6/mL BAL)	0.053 ± 0.011	0.068 ± 0.021	0.128 ± 0.031*
Neutrophils (x10^6/mL BAL)	0.065 ± 0.013	0.031 ± 0.010	0.653 ± 0.311
Eosinophils (x10^6/mL BAL)	0.002 ± 0.000	0.039 ± 0.017	0.050 ± 0.019*
ICS, yes/no	NA	9/3	11/0
ICS dose$^{\$}$	NA	543.30 ± 126.70	800.00 ± 80.90
LABA, yes/no	NA	6/6	11/0
LAMA, yes/no	NA	4/8	5/6
SABA, yes/no	NA	5/7	5/6
OCS, yes/no	NA	0/12	2/9

M/F, male/female; BMI, body mass index; FEV1, forced expiratory volume in one second; FVC, forced vital capacity; ACQ, asthma control questionnaire; BAL, bronchoalveolar lavage; NA, not applicable; ICS, inhaled corticosteroids; LABA, long-acting β2-agonist; LAMA, long-acting muscarinic antagonist; SABA, short-acting β-agonist; OCS, oral corticosteroids; yr, year. $^{\$}$Equivalent to Fluticasone μg/day. Data are shown as mean ± SEM. $^{*}p<0.05$, $^{**}p<0.01$, $^{***}p<0.001$ compared to healthy controls; $^{\#}p<0.05$, $^{\#\#}p<0.01$ compared to mild-moderate asthmatics

Table 2.

Characteristic	Healthy	Mild-moderate asthmatics	Severe asthmatics
Number of subjects, n	10	10	10
Age, yr	58.56 ± 2.724	60.70 ± 5.327	56.00 ± 3.841
Sex, M/F	4/6	5/5	5/5
FEV1% predicted	97.5 ± 5.861	89.6 ± 4.759	66.33 ± 7.427$^{**, \#}$
FEV1/FVC	0.812 ± 0.008	0.741 ± 0.023*	0.745 ± 0.035
ACQ	-	4.778 ± 0.8127	7.333 ± 3.18
Total cells (x10^6/mL BAL)	0.110 ± 0.028	0.138 ± 0.027	0.126 ± 0.016
Macrophages (x10^6/mL BAL)	0.037 ± 0.009	0.031 ± 0.008	0.051 ± 0.013
Neutrophils (x10^6/mL BAL)	0.025 ± 0.009	0.053 ± 0.022	0.039 ± 0.008
Eosinophils (x10^6/mL BAL)	0.000 ± 0.000	0.020 ± 0.011	0.029 ± 0.012
ICS, yes/no	NA	8/2	10/0
ICS dose$^{\$}$	NA	432.0 ± 110.4	1063 ± 174.2
LABA, yes/no	NA	5/5	10/0
LAMA, yes/no	NA	2/8	6/4
SABA, yes/no	NA	4/6	4/6
OCS, yes/no	NA	0/10	0/10

M/F, male/female; BMI, body mass index; FEV1, forced expiratory volume in one second; FVC, forced vital capacity; ACQ, asthma control questionnaire; BAL, bronchoalveolar lavage; NA, not applicable; ICS, inhaled corticosteroids; LABA, long-acting β2-agonist; LAMA, long-acting muscarinic antagonist; SABA, short-acting β-agonist; OCS, oral corticosteroids; yr, year. $^{\$}$Equivalent to Fluticasone μg/day. Data are shown as mean ± SEM. $^{*}p<0.05$, $^{**}p<0.01$, compared to healthy controls; $^{\#}p<0.05$ compared to mild-moderate asthmatics.

Supplementary Methods

Study approvals

All experiments were conducted with approval of the Human/Animal Research Ethics Committees of the University of Newcastle, Australia and the Unbiased Biomarkers in Prediction of respiratory disease outcomes (U-BIOPRED) centre.

Human subjects

Airway biopsy tissues and bronchoalveolar lavage (BAL) were collected from 11 severe, 12 mild-moderate asthmatics and 13 healthy subjects. To measure non-haem iron content in BAL supernatant, BAL samples were also collected from a second set of severe or mild-moderate asthma patients and healthy subjects (10 subjects in each group). Subjects with severe or mild-moderate asthma had mean FEV1% predicted at 86.92 ± 2.726 (p0.01) and 76 ± 5.389 (p0.001), respectively, compared to healthy controls (102.7 ± 4.494, **Table 1**). BAL was collected from another set of 10 subjects in each group: severe (mean FEV1% predicted, 66.33 ± 7.427, p<0.01) or mild-moderate asthma (mean FEV1%, 89.6 ± 4.759) or healthy controls (mean FEV1%, 97.5 ± 5.861) (**Table 2**). Human bronchial airway epithelial cells (pBECs), airway smooth muscle (ASM) cells and lung fibroblasts donor characteristics are shown in **Tables E5 and 6**. Patient exclusion criteria included current smokers, recent exacerbation, respiratory tract infection in the last 4 weeks and age younger than 18yrs.

Human BAL

For each donor, BAL was collected by instilling sterile warm saline (2x 60mL) into the airways using elective fibreoptic bronchoscopy, as described previously (1). Collected BAL was

filtered through a nylon filter apparatus, centrifuged (400x *g*, 10 mins) and then supernatant was stored at −80°C for future analysis. BAL cell pellets were resuspended in PBS and cytospins were prepared, stained with Diff-quik solutions for 30 sec, solution II (fixative) for 30 sec, solution I for 30 sec, dehydrated and air-dried overnight for cover slipping. Differential cells were analysed based on morphology as previously described (1).

Quantification of iron-laden BAL cells

Total iron positive cells and iron score index levels were calculated by enumerating the different grade of iron scored cells (Grade 0, 1, 2 and 3) using Perls'-DAB stained (*see below*) BAL cytospins.

Mouse models of iron overload

We utilised two models of iron overload to assess the effects of iron on asthma. We first used female *Hfe*$^{-/-}$ and WT mice (36 weeks old) (2) on an AKR background strain that were fed a normal diet. Disruption of this gene results in deficiency in hepcidin production, leading to increased systemic iron levels (2-4). In addition, female BALB/c mice (6-8 weeks of age) were fed a diet of mouse chow that contains 2% carbonyl iron (19410mg Fe/Kg diet, Specialty Feeds, Western Australia) *ad libitum* for 8 weeks. This results in a similar level of iron load in the liver as *Hfe*$^{-/-}$ mice. WT BALB/c mice were also maintained on control iron diet (~49 mg Fe/Kg diet) or low iron diet (~2.5mg Fe/Kg diet, Speciality Feeds, Western Australia) for 8 weeks as a comparison. All mice were housed at 22 ± 2° temperature with humidity range of 30-70 under 12 hours dark/light cycling conditions.

HDM-induced chronic experimental asthma

WT AKR and *Hfe*$^{-/-}$ female mice (~36 weeks old), and WT BALB/c female mice (8 weeks old) fed low iron, control and high iron diets were intranasally administered HDM extract (25µg, 50 µl PBS, Greer Laboratories, Lenoir, NC) or vehicle (PBS) 5 days per week for 6 weeks. After 6 weeks, liver and lung tissues were collected for further analysis, and AHR was measured.

Perls' and DAB-enhanced Perls' stain

The single lobed lungs from mice were perfused with saline, inflated and fixed with formalin, paraffin-embedded, and sectioned (4-6µm). Sections were deparaffinised with xylene and a graded series of ethanol. Deparaffinised mouse lung sections or BAL cell cytospins prepared from clinical and experimental samples were submerged in fresh 1% Potassium Ferrocyanide (AnalaR), pH 1 (Perls' solution), for 30 min on a shaker. Each slide was washed briefly in distilled water, incubated in methanol containing 0.01M NaN_3 (MERCK) and 0.3% H_2O_2 for 1 h on a shaker. Slides were rinsed in 0.1M PBS (pH7.4) and iron staining was enhanced by 1 h of incubation with 0.025% 3, 3'-Diaminobenzidine-4HCl (DAB, MP Biomedical) and 0.005% H_2O_2 in 0.1M PBS (pH 7.4) on a shaker. Slides were then washed in distilled water, dehydrated with a series of graded ethanol, cleared with xylene, and cover slipped using DEPEX mounting medium (BDH Chemical).

Non-haem iron assay for the assessment of iron levels in BAL supernatants and tissue

Non-haem iron content in BAL supernatants from severe or mild-moderate asthma patients or healthy controls, and in murine liver and lung tissues were measured as previously described (5). For the latter, briefly, ~50mg of wet tissues of liver or lung were homogenised in 1 ml of 0.9% NaCl solution on ice. Iron standard solutions ranging in concentration from 0 to 8µg/ml

were prepared from a stock solution of 5mM $FeSO_4$ (BDH Chemical). Then 100µl of iron standards or BAL supernatant or tissue homogenates were mixed with 50µL of 3.8M (12%) HCl and incubated at 85°C for 30 min. Then, 25µL of 50% trichloroacetic acid (Sigma-Aldrich, Australia) was added into each tube followed by incubated on ice for 10 min. After centrifugation (235 xg, room temperature, 20 min), 100 µl of supernatant was removed from each tube and added in triplicate to clear 96-well plates. Finally, 100µl of colour reagent (816µM bathophenanthroline disulfonic acid, 1.9M sodium acetate, 0.2% (v/v) thioglycolic acid; Sigma) was added to each well to develop colour and absorbance was measured at 560nm using a microplate reader (Synergy2, Millennium Science). After subtracting absorbance of blank samples, iron concentrations were calculated from the standard curve.

Gene expression analysis by RT-qPCR

Total RNA was extracted from frozen mouse lung tissues using Trizol reagent (Invitrogen, Life Technologies, Australia) as described previously (6). Mouse total RNA (1µg) was reverse transcribed into cDNA using Bioscript (Bioline, Australia) and random hexamer primers (Invitrogen, Life Technologies, Australia). For human airway biopsy tissues, total RNA was isolated using QIAGEN RNeasy Mini kit for human airway biopsy tissue homogenates (Qiagen, Venlo, Netherlands, Cat# 990394) according to the manufacturer's instructions. Human cDNA was collected using a reverse transcription kit (Applied Biosystems, USA). The level of mRNA transcripts for iron regulatory molecules and cytokines were measured by SYBR-green qPCR using Eppendorf RealPlex (Eppendorf, Germany) and relative expression was normalised to transcripts of *HPRT* (mouse gene expression) or beta actin (human gene expression) (7-9). The formula used for calculating relative expression of each gene of interest was $2^{-(\text{Ct gene of interest - Ct HPRT})}$ (10). Primer sequences are shown in **Tables E1 and 2**. Total mRNA from primary human ASM cells and lung fibroblast culture experiments was isolated using the

ISOLATE II RNA Mini Kit and transcribed into cDNA using the SensiFAST™ cDNA Synthesis Kit (Bioline, Alexandria, Australia), according to the manufacturer's instructions. Assays were carried out in triplicate using a reaction mixture containing the Bioline SensiFAST Probe Hi-ROX Master Mix and TaqMan primer sets for *TNC* (Hs01115665_m1) and the ubiquitously expressed ribosomal RNA (18S rRNA) as a housekeeping gene. qPCR was performed using the StepOnePlus detection system and data were collected and analysed by StepOne software (Applied Biosystems, Melbourne, Australia).

Mouse BAL

BAL collection, processing and cytospin preparations were performed as described previously (11). BAL cells cytospin slides were stained with May-Grunwald-Giemsa, differential immune cells were counted (≈175) using light microscopy at 40x magnification based on key morphological characteristics (12, 13).

Lung tissue eosinophil and airway mucus-secreting cell numbers

Lung sections were deparaffinised and stained with chrome salt fixation (for eosinophils) or periodic acid–Schiff (for mucus-secreting cells). Numbers of eosinophils and PAS positive cells (i.e. mucus secreting cells) were counted per 100µm around the airways at 100x magnification as previously described (12, 13).

Small airway remodelling

Airway remodelling in terms of collagen thickness around the small airways was evaluated in at least 6 small airway images (40x magnification) from Sirius Red and Fast Green-stained (Sigma Aldrich, USA) mouse lung sections using ImageJ (version 1.47, Media Cybernetics, Rockville, MD, USA) as previously described (11).

AHR

AHR in terms of central airway resistance (Rn) in response to nebulised methacholine (MCh) was measured using FlexiVent apparatus (FX1 System; SCIREQ, Montreal, Canada). Briefly, mice were anaesthetised with a mixture of ketamine (100mg/kg, Parnell)) and xylazine (10mg/kg, Troy Laboratories, Smithfield, Australia). Following tracheostomy, cannulae were inserted into their tracheas and ligated (7, 12-14). Rn (tidal volume of 8mL/kg at a respiratory rate of 450 breaths/min) was measured in response to increasing doses of nebulised MCh (up to 30mg/kg; Sigma-Aldrich, Sydney, Australia) (14).

IL6, IL8 and transferrin detection. Levels of IL-6 and IL-8 in cell-free supernatants were measured by sandwich ELISA, using commercial antibody kits according to the manufacturer's instructions (R&D Systems, MN). The detection limit of both assays was 15.6 pg/ml. Levels of transferrin in BAL supernatants were measured using commercial ELISA kit according to the manufacturer's instructions (Abcam: ab157724).

Flow cytometric analysis of macrophage populations in murine lung tissue. Flow cytometry was performed on murine whole lung single cell suspensions to determine the number and activation of macrophage subsets (15). Lung tissue was processed into single cell suspensions *via* enzymatic digestion with collagenase D (2mg/mL, Roche, Sydney, Australia), DNase I (400U/mL, Roche) and a gentleMACS™ Dissociator (Miltenyi Biotec). Total lungs cells were collected, and red blood cells lysed (155mM NH_4Cl, 12mM $NaHCO_3$, 0.1mM ethylenediaminetetraacetic acid [EDTA], pH 7.35, 5mins, 4°C). Total cell counts were performed using a haemocytometer under a light microscope (20x magnification) and trypan blue (Sigma-Aldrich) exclusion. Total cells stained with fluorescently conjugated antibodies

specific for CD45, F4/80, CD11c, CD11b, Ly6C, SiglecF and TFR1 (**Table E3)** (BD Biosciences, San Diego, USA; Biolegend, San Diego, USA). Live cell discrimination was assessed with Zombie yellow fixable viability dye (Biolegend). Cells were then analysed using a LSR Fortessa X-20 (BD Biosciences) and FACSDiva software (BD Biosciences). After exclusion of cell debris, doublets and dead cells, macrophage subsets were determined based on antigen expression (**Table E4**).

Isolation of macrophages from whole lung tissue. Lungs were processed into single cell suspensions and stained with fluorochrome-conjugated antibodies as above. $Tfr1^+$ macrophages were isolated by fluorescence-activated cell sorting using an ARIA III (BD Biosciences) into PBS with 5% FCS.

RNA extraction from isolated macrophages and reverse transcription (RT). Total RNA was extracted from sorted $Tfr1^+$ macrophages using miRNeasy mini kit (Qiagen, Chadstone, Australia) as per manufacturer's instructions. Sorted cells were collected into Qiazol® (750µL) and stored at -80°C until RNA extraction. Upon thawing of cells, chloroform (140 µL) was added and vortexed prior to phase separation by centrifugation (15min, 4˚C, 12,000x*g*). The aqueous phase was collected before automated RNA extraction using Qiacube apparatus (Qiagen). This automated protocol supplemented samples with 100% molecular grade ethanol prior to centrifugation. Samples were transferred to spin columns and washed with RWT buffer. RPE buffer was added to columns prior to further centrifugation. Purified RNA was eluted using RNAse-free water. RNA purity and concentration were determined using a NanoDrop™ 1000 Spectrophotometer (Thermo Fisher Scientific, North Ryde, Australia). The 260/230nm and 260/280nm absorption ratios accepted as pure RNA was >1.90, and >2.00, respectively. RNA from isolated macrophages was reverse transcribed to cDNA

using the miScript II RT kit (Qiagen) as per manufacturer's instructions. Samples were supplemented with miScript HiFlex buffer (4µl), 10x miScript Nucleics mix (2µl) and miScript reverse transcriptase mix (2µl). Reverse transcription was achieved using a Bio-Rad T100 Thermal Cycler (60min, 37°C; 5min, 95°C). Samples were then stored at -20°C until quantification by qPCR.

ASM cell and lung fibroblasts culture. Primary human ASM cells and lung fibroblasts were isolated from the parenchyma of lungs from patients undergoing lung transplantation as previously described (16). Patient demographics are described in **Table E6**. Cells were seeded in 12 or 96 well plates at 4.5×10^4 cells/mL in DMEM with 5% fetal bovine serum and 1% antibiotic-antimycotic, and cultured to near confluence (72h, 37°C, 5% CO_2). Cells were serum starved in DMEM with 0.1% bovine serum albumin for 24h prior to stimulation. Cells were stimulated with a range of ferric ammonium citrate (FAC) concentrations for 48h, with additions replenished at 24h. Cell free supernatants or total RNA lysates were collected at 48h and stored at -20°C for analysis. All experiments were carried out using fibroblasts between passage 2 and 4.

Primary bronchial airway epithelial cells (pBECs) cultured at the air-liquid interface (ALI) (17). Human pBECs were obtained from healthy controls, and patients with severe asthma. pBECs were raised and maintained in placental collagen-coated T75 tissue culture flasks (Interpath, Australia) with Bronchial Epithelial Cell Growth Medium (BEGM™, Lonza, USA), supplemented with BEGM™ SingleQuots™ supplements and Growth Factors (BEGM™ BulletKit™, Lonza), penicillin/streptomycin (Life Technologies, USA) and amphotericin B (Sigma, USA). Cell monolayers at 70%-80% confluency were detached with 1:10 trypsin-ethylenediaminetetraacetic acid/Dulbecco's phosphate buffered saline (1:10

trypsin-EDTA/D-PBS, 4mL). Trypsin enzyme activity was neutralised with foetal bovine serum (FBS) and cells were resuspended in ALI initial medium. Detached cells were then enumerated and seeded at $2x10^5$ cells/500µL initial media onto the apical compartment of a 12-well plate (Corning, USA) containing a 12mm polyester membrane transwell (0.4µm pore size, Sigma). ALI initial media was also added to the basal compartment (1.5mL/well) and refreshed (1.5mL/well) 24h after seeding. At 72h post-seeding, all apical media was removed and basal media replaced with ALI final medium (1.5mL/well). This timepoint was demarcated as "day 0" of ALI culture and the beginning of the experimental period. Basolateral media was replaced every two days with 1.5mL fresh ALI final medium. Apical surfaces of the ALI cultures were washed with sterile 1xD-PBS (500uL/well) weekly, and trans-epithelial electrical resistance measured (Epithelial Volt/ohmmeter 2 [$EVOM_2$], Coherent Scientific) to track monolayer formation. This weekly apical wash also served to remove any mucus build-up from the cultures. Patient cells were grown at ALI in culture conditions (37°C, 5% CO_2) for 28 days to ensure maximal differentiation. Following sufficient differentiation of the cells basal media was replaced with ALI minimal media (1.5 mL/well) and incubated overnight (37°C, 5% CO_2). Apical compartments of each well were then supplemented with minimal media and 1xD-PBS (500uL) and basal minimal media was replaced (1.5mL) prior to the second overnight incubation (37°C, 5% CO_2). At the end of the protocol, apical and basal media was removed and stored at -80°C for further analysis. Cells from the apical ALI membrane insert were also harvested and stored in Qiazol® lysis reagent (700uL, Qiagen, -80°C) for further processing.

Statistics

Comparisons between two groups were performed using a non-parametric Mann-Whitney test. Comparisons between multiple groups were performed using Kruskal-Wallis one-way analysis of variance (ANOVA) with uncorrected Dunn's post-hoc test. AHR data were analysed using

two-way repeated measures ANOVA with Bonferroni post-hoc test. Correlation analyses were performed using Spearman rank correlation. All statistical analysis was performed using GraphPad Prism V.7 Software (San Diego, California, USA).

Supplementary results

HDM-induced experimental asthma

Intranasal HDM-treatment increases the number of immune cells (macrophages, neutrophils, eosinophils) in BAL, airway tissue eosinophil numbers, mucus secreting cell numbers, and collagen deposition in airway tissue and this is associated with increased airway hyper-responsiveness (AHR) (**Figure E2 A-F**).

Supplementary discussion

We show a significant increase in iron positive BAL cells in subjects with severe and mild-moderate asthma compared to healthy controls. Increased numbers of iron-laden cells have been reported in patients with COPD (18), IPF (19) and cigarette smokers (20). The increased iron in the lung of cigarette smokers may not be dyshomeostasis, but actual loading of lungs with additional iron on inhalation. However, these findings do suggest that increased numbers of iron laden cells in the airways is a key feature of several lung diseases. Our data is also consistent, with a recent case report where haemosiderin-laden macrophages were identified in BAL from an 8-year old child with recurrent iron-deficiency anaemia (IDA) and allergic asthma and later diagnosed with idiopathic pulmonary haemosiderosis (IPH) (21). However,

since this study is based on a single patient it is unclear whether IDA and/or macrophage haemosiderin are associated with allergic asthma or IPH.

To protect from the potentially harmful effects of excess free iron, iron regulatory systems must be tightly regulated in the body. Although little is known about the iron metabolism in the lung, as with other organs, iron homeostasis in the lung is maintained by a range of iron regulatory molecules, including iron uptake (transferrin receptors, TFR1, TFR2); divalent metal transporter 1 (DMT1); zinc transporter protein 14 (ZIP14); natural resistance-associated macrophage protein 1 (NRAMP1) and lactoferrin receptor (LFR); transport (Transferrin, TF), storage (ferritin heavy and light chain, FTH, FTL) and export (ferroportin, FPN) from cells. Iron-responsive proteins (IRPs) control the expression of these genes through binding with the 5′ or 3′ untranslated regions of these genes mRNA (22).

We show that *NRAMP1* expression is higher in the airways of mild-moderate asthma patients and tends to further increase in severe asthma compared to healthy controls (**Figure 3C**). NRAMP1 has been reported to affect IgE responses, the development of Th2 cell responses and mast cell degranulation in ovalbumin-induced allergic asthma in mice (23). We also show increased *TFR2* in the airways of severe asthma patients (**Figure 3A**). TFR2 acts as an iron sensor of transferrin-bound iron (Fe-TF) that stimulates hepcidin production (24). In addition, ZIP14 levels have been shown to increase in airway cells in iron overload and decrease in iron deficiency in mice (25). We show increased *FTH* and *IRP1* expression in airways of mild-moderate but not severe asthma patients (**Figure 3D, F**). Furthermore, *FTL* expression reduced (p=0.06) in the airways of severe compared to mild-moderate asthma patients (**Figure 3E**). Another study suggested that *FTL* has anti-inflammatory effects, which agree with our findings (26). In addition, we find that the only known iron exporter, *FPN* expression is not altered in asthma (**Figure 3H**). All these data provide strong evidence that

317 there is an environment of increased iron sequestration into cells in asthmatic airways that leads
318 to increased cellular but reduced extracellular iron levels in BAL in asthma.

319 To explore the relationship between iron and asthma, we performed a series of studies
320 to determine the effects of LID on key disease features. Decreasing systemic iron levels using
321 a LID had no effect on lung iron levels but increased AHR in the absence of HDM-induced
322 experimental asthma. However, we also show that a LID reduces iron accumulation in HDM-
323 induced experimental asthma and protects against some of the key features of disease. These
324 findings highlight the complexity and importance of systemic:local iron regulatory interactions
325 in the pathogenesis of asthma, and also demonstrates that both low and high systemic iron may
326 promote/increase the severity of key disease features in different contexts, which is consistent
327 with the controversy in the literature (27-32).

328 Whilst our findings demonstrate that increased iron accumulation in cells and tissues in
329 the airways and lung is linked to key features of asthma and plays a role in the worsening of
330 lung function and disease severity, they do not elucidate the underlying mechanisms involved
331 in iron-mediated effects. A large body of evidence suggests that iron-induced oxidative stress
332 may play a key role (24). Iron accumulation has been suggested to induce oxidative stress and
333 contribute to the pathogenesis of Alzheimer's disease, atherosclerosis and Parkinson's disease
334 (33), and there is a clear involvement of oxidative stress in asthma (34, 35). Increased
335 production of ROS and reactive nitrogen species (RNS) and reduced or inactivated antioxidant
336 responses occur in patients with bronchial asthma (36-40). Lipid peroxidation in plasma and
337 exhaled breath condensate (EBC) is inversely correlated with airflow obstruction in asthma
338 (41). In addition, total antioxidant capacity in plasma and sputum, and SOD levels in plasma
339 and airway epithelial cells (AEC) have been reported to be positively associated with airflow
340 obstruction in asthmatics (41). Chronic inflammation can generate ROS (42), and
341 overproduction of ROS/RNS reportedly leads to airway inflammation and remodelling, mucus

342 overproduction, tissue injury and lung function decline in clinical and experimental asthma
343 studies (43, 44). Notably, a significant increase in iron and MDA levels in plasma have been
344 shown in asthmatics, and there is a positive correlation between MDA and iron levels (32),
345 suggesting that increased systemic iron may promote asthma. Furthermore, increased levels of
346 oxidative stress (increased MDA, catalase, SOD, GPX and nitrotyrosine levels) and
347 inflammatory responses (increased HIF1α, NF-κB and TNFα levels) with increased iron
348 accumulation in the lung have been shown in rats treated with low molecular weight iron
349 dextran (45). Based on this evidence, increased iron may drive disease through increased
350 oxidative stress in tissues that drives many of the key features of disease.

351 Ferroptosis, a process of iron-dependent programmed cell death, has recently been
352 suggested to be a key molecular mechanisms implicated in kidney, brain, liver, heart and lung
353 pathology (46-51). Recently, Wenzel *et al.*, uncovered evidence for phosphatidylethanolamine-
354 binding protein 1 (PEBP1)-dependent regulatory mechanisms of ferroptotic death in AEC in
355 asthma (52). Since we show that experimental asthma results in increased iron accumulation
356 in lung cells and tissues as well as evidence for increased iron sequestration in clinical airway
357 samples, it is possible that increased iron accumulation-mediated ferroptotic cell death may
358 contribute to disease pathogenesis. However, further studies are required to explore
359 mechanisms of the association between iron and ferroptosis in asthma pathogenesis and to
360 determine the $Fe^{2+/3+}$ status and localisation within airway cells.

361 In the lung, iron can also be derived from non-dietary sources e.g smoking, pollution
362 or geogenic iron. Increased iron accumulation in the lung as a result of these exogenous
363 exposures may also contribute to lung pathology. Indeed, Indeed, a recent study has shown that
364 increased concentrations of iron in particulate matter result in lung impairment 7 days-post
365 intranasal exposure in mice (53). It is also important to note that infections are associated with
366 the development of asthma phenotypes and that humans and mice with asthma or allergic

airway disease have altered microbiomes and predispose to respiratory infections that increase the severity or exacerbate their disease (24) . Excess iron can also increase susceptibility to respiratory infections (24), which may modify the immune system and promote disease pathogenesis.

Due to the limited availability of appropriate airway tissue samples, and the prospective nature of our analyses, we needed to draw bronchoscopy samples from two different cohorts. We note that there was no significant difference in asthma control questionnaire (ACQ) and BAL cellular profiles in the cohorts that we used for BAL non-haem iron studies. Our findings from these two different cohorts highlight that iron levels and regulation are altered in asthma.

References

1. Vlahos R, Wark PA, Anderson GP, Bozinovski S. Glucocorticosteroids differentially regulate MMP-9 and neutrophil elastase in COPD. *PLoS One* 2012; 7: e33277.
2. Zhou XY, Tomatsu S, Fleming RE, Parkkila S, Waheed A, Jiang J, Fei Y, Brunt EM, Ruddy DA, Prass CE, Schatzman RC, O'Neill R, Britton RS, Bacon BR, Sly WS. HFE gene knockout produces mouse model of hereditary hemochromatosis. *Proc Natl Acad Sci U S A* 1998; 95: 2492-2497.
3. Gao J, Chen J, De Domenico I, Koeller DM, Harding CO, Fleming RE, Koeberl DD, Enns CA. Hepatocyte-targeted HFE and TFR2 control hepcidin expression in mice. *Blood* 2010; 115: 3374-3381.
4. Schmidt PJ, Toran PT, Giannetti AM, Bjorkman PJ, Andrews NC. The transferrin receptor modulates Hfe-dependent regulation of hepcidin expression. *Cell Metab* 2008; 7: 205-214.

5. Kaldor I. Studies on intermediary iron metabolism. V. The measurement of non-haemoglobin tissue iron. *Aust J Exp Biol Med Sci* 1954; 32: 795-799.

6. Collison A, Hatchwell L, Verrills N, Wark PA, de Siqueira AP, Tooze M, Carpenter H, Don AS, Morris JC, Zimmermann N, Bartlett NW, Rothenberg ME, Johnston SL, Foster PS, Mattes J. The E3 ubiquitin ligase midline 1 promotes allergen and rhinovirus-induced asthma by inhibiting protein phosphatase 2A activity. *Nat Med* 2013; 19: 232-237.

7. Beckett EL, Stevens RL, Jarnicki AG, Kim RY, Hanish I, Hansbro NG, Deane A, Keely S, Horvat JC, Yang M, Oliver BG, van Rooijen N, Inman MD, Adachi R, Soberman RJ, Hamadi S, Wark PA, Foster PS, Hansbro PM. A new short-term mouse model of chronic obstructive pulmonary disease identifies a role for mast cell tryptase in pathogenesis. *J Allergy Clin Immunol* 2013; 131: 752-762.

8. Essilfie AT, Horvat JC, Kim RY, Mayall JR, Pinkerton JW, Beckett EL, Starkey MR, Simpson JL, Foster PS, Gibson PG, Hansbro PM. Macrolide therapy suppresses key features of experimental steroid-sensitive and steroid-insensitive asthma. *Thorax* 2015; 70: 458-467.

9. Asquith KL, Horvat JC, Kaiko GE, Carey AJ, Beagley KW, Hansbro PM, Foster PS. Interleukin-13 promotes susceptibility to chlamydial infection of the respiratory and genital tracts. *PLoS Pathog* 2011; 7: e1001339.

10. Horvat JC, Starkey MR, Kim RY, Phipps S, Gibson PG, Beagley KW, Foster PS, Hansbro PM. Early-life chlamydial lung infection enhances allergic airways disease through age-dependent differences in immunopathology. *J Allergy Clin Immunol* 2010; 125: 617-625, 625 e611-625 e616.

11. Liu G, Cooley MA, Jarnicki AG, Hsu AC, Nair PM, Haw TJ, Fricker M, Gellatly SL, Kim RY, Inman MD, Tjin G, Wark PA, Walker MM, Horvat JC, Oliver BG, Argraves WS,

414 Knight DA, Burgess JK, Hansbro PM. Fibulin-1 regulates the pathogenesis of tissue
415 remodeling in respiratory diseases. *JCI Insight* 2016; 1.
416 12. Horvat JC, Beagley KW, Wade MA, Preston JA, Hansbro NG, Hickey DK, Kaiko GE,
417 Gibson PG, Foster PS, Hansbro PM. Neonatal chlamydial infection induces mixed T-
418 cell responses that drive allergic airway disease. *Am J Respir Crit Care Med* 2007; 176:
419 556-564.
420 13. Horvat JC, Starkey MR, Kim RY, Beagley KW, Preston JA, Gibson PG, Foster PS,
421 Hansbro PM. Chlamydial respiratory infection during allergen sensitization drives
422 neutrophilic allergic airways disease. *J Immunol* 2010; 184: 4159-4169.
423 14. Kim RY, Horvat JC, Pinkerton JW, Starkey MR, Essilfie AT, Mayall JR, Nair PM, Hansbro
424 NG, Jones B, Haw TJ, Sunkara KP, Nguyen TH, Jarnicki AG, Keely S, Mattes J,
425 Adcock IM, Foster PS, Hansbro PM. MicroRNA-21 drives severe, steroid-insensitive
426 experimental asthma by amplifying phosphoinositide 3-kinase-mediated suppression of
427 histone deacetylase 2. *J Allergy Clin Immunol* 2017; 139: 519-532.
428 15. Starkey MR, Nguyen DH, Brown AC, Essilfie AT, Kim RY, Yagita H, Horvat JC, Hansbro
429 PM. Programmed Death Ligand 1 Promotes Early-Life Chlamydia Respiratory
430 Infection-Induced Severe Allergic Airway Disease. *Am J Respir Cell Mol Biol* 2016;
431 54: 493-503.
432 16. Krimmer D, Ichimaru Y, Burgess J, Black J, Oliver B. Exposure to biomass smoke extract
433 enhances fibronectin release from fibroblasts. *PLoS One* 2013; 8: e83938.
434 17. Hsu AC, Starkey MR, Hanish I, Parsons K, Haw TJ, Howland LJ, Barr I, Mahony JB,
435 Foster PS, Knight DA, Wark PA, Hansbro PM. Targeting PI3K-p110alpha Suppresses
436 Influenza Virus Infection in Chronic Obstructive Pulmonary Disease. *Am J Respir Crit*
437 *Care Med* 2015; 191: 1012-1023.

438 18. Philippot Q, Deslee G, Adair-Kirk TL, Woods JC, Byers D, Conradi S, Dury S, Perotin
439 JM, Lebargy F, Cassan C, Le Naour R, Holtzman MJ, Pierce RA. Increased iron
440 sequestration in alveolar macrophages in chronic obstructive pulmonary disease. *PLoS*
441 *One* 2014; 9: e96285.
442 19. Sangiuolo F, Puxeddu E, Pezzuto G, Cavalli F, Longo G, Comandini A, Di Pierro D,
443 Pallante M, Sergiacomi G, Simonetti G, Zompatori M, Orlandi A, Magrini A,
444 Amicosante M, Mariani F, Losi M, Fraboni D, Bisetti A, Saltini C. HFE gene variants
445 and iron-induced oxygen radical generation in idiopathic pulmonary fibrosis. *Eur*
446 *Respir J* 2015; 45: 483-490.
447 20. Thompson AB, Bohling T, Heires A, Linder J, Rennard SI. Lower respiratory tract iron
448 burden is increased in association with cigarette smoking. *J Lab Clin Med* 1991; 117:
449 493-499.
450 21. Eldem I, Ileri T, Ince E, Asarcikli F, Pekpak E, Cakmakli HF, Ceyhan K, Uysal Z.
451 Idiopathic Pulmonary Hemosiderosis With Allergic Asthma Diagnosis in a Pediatric
452 Patient. *J Pediatr Hematol Oncol* 2015; 37: e435-437.
453 22. Wang J, Pantopoulos K. Regulation of cellular iron metabolism. *Biochem J* 2011; 434: 365-
454 381.
455 23. Smit JJ, van Loveren H, Hoekstra MO, Nijkamp FP, Bloksma N. Influence of the
456 macrophage bacterial resistance gene, Nramp1 (Slc11a1), on the induction of allergic
457 asthma in the mouse. *FASEB J* 2003; 17: 958-960.
458 24. Ali MK, Kim RY, Karim R, Mayall JR, Martin KL, Shahandeh A, Abbasian F, Starkey
459 MR, Loustaud-Ratti V, Johnstone D, Milward EA, Hansbro PM, Horvat JC. Role of
460 iron in the pathogenesis of respiratory disease. *Int J Biochem Cell Biol* 2017; 88: 181-
461 195.

462 25. Giorgi G, D'Anna MC, Roque ME. Iron homeostasis and its disruption in mouse lung in
463 iron deficiency and overload. *Exp Physiol* 2015; 100: 1199-1216.
464 26. Fan Y, Zhang J, Cai L, Wang S, Liu C, Zhang Y, You L, Fu Y, Shi Z, Yin Z, Luo L, Chang
465 Y, Duan X. The effect of anti-inflammatory properties of ferritin light chain on
466 lipopolysaccharide-induced inflammatory response in murine macrophages. *Biochim*
467 *Biophys Acta* 2014; 1843: 2775-2783.
468 27. Ramakrishnan K, Borade A. Anemia as a risk factor for childhood asthma. *Lung India*
469 2010; 27: 51-53.
470 28. Vlasic Z, Dodig S, Cepelak I, Topic RZ, Zivcic J, Nogalo B, Turkalj M. Iron and ferritin
471 concentrations in exhaled breath condensate of children with asthma. *J Asthma* 2009;
472 46: 81-85.
473 29. Brigham EP, McCormack MC, Takemoto CM, Matsui EC. Iron status is associated with
474 asthma and lung function in US women. *PLoS One* 2015; 10: e0117545.
475 30. Ekmekci OB, Donma O, Sardogan E, Yildirim N, Uysal O, Demirel H, Demir T. Iron, nitric
476 oxide, and myeloperoxidase in asthmatic patients. *Biochemistry (Mosc)* 2004; 69: 462-
477 467.
478 31. Kocyigit A, Armutcu F, Gurel A, Ermis B. Alterations in plasma essential trace elements
479 selenium, manganese, zinc, copper, and iron concentrations and the possible role of
480 these elements on oxidative status in patients with childhood asthma. *Biol Trace Elem*
481 *Res* 2004; 97: 31-41.
482 32. Narula MK, Ahuja GK, Whig J, Narang AP, Soni RK. Status of lipid peroxidation and
483 plasma iron level in bronchial asthmatic patients. *Indian J Physiol Pharmacol* 2007;
484 51: 289-292.
485 33. Altamura S, Muckenthaler MU. Iron toxicity in diseases of aging: Alzheimer's disease,
486 Parkinson's disease and atherosclerosis. *J Alzheimers Dis* 2009; 16: 879-895.

487 34. Ruprai RK. Plasma oxidant-antioxidants status in asthma and its correlation with
488 pulmonary function tests. *Indian J Physiol Pharmacol* 2011; 55: 281-287.
489 35. Sagdic A, Sener O, Bulucu F, Karadurmus N, Ozel HE, Yamanel L, Tasci C, Naharci I,
490 Ocal R, Aydin A. Oxidative stress status and plasma trace elements in patients with
491 asthma or allergic rhinitis. *Allergol Immunopathol (Madr)* 2011; 39: 200-205.
492 36. Iyer D, Mishra N, Agrawal A. Mitochondrial Function in Allergic Disease. *Curr Allergy*
493 *Asthma Rep* 2017; 17: 29.
494 37. Calhoun WJ, Reed HE, Moest DR, Stevens CA. Enhanced superoxide production by
495 alveolar macrophages and air-space cells, airway inflammation, and alveolar
496 macrophage density changes after segmental antigen bronchoprovocation in allergic
497 subjects. *Am Rev Respir Dis* 1992; 145: 317-325.
498 38. Comhair SA, Xu W, Ghosh S, Thunnissen FB, Almasan A, Calhoun WJ, Janocha AJ,
499 Zheng L, Hazen SL, Erzurum SC. Superoxide dismutase inactivation in
500 pathophysiology of asthmatic airway remodeling and reactivity. *Am J Pathol* 2005;
501 166: 663-674.
502 39. Smith LJ, Shamsuddin M, Sporn PH, Denenberg M, Anderson J. Reduced superoxide
503 dismutase in lung cells of patients with asthma. *Free Radic Biol Med* 1997; 22: 1301-
504 1307.
505 40. Jesenak M, Zelieskova M, Babusikova E. Oxidative Stress and Bronchial Asthma in
506 Children-Causes or Consequences? *Front Pediatr* 2017; 5: 162.
507 41. Nadeem A, Siddiqui N, Alharbi NO, Alharbi MM. Airway and systemic oxidant-
508 antioxidant dysregulation in asthma: a possible scenario of oxidants spill over from
509 lung into blood. *Pulm Pharmacol Ther* 2014; 29: 31-40.
510 42. Andreadis AA, Hazen SL, Comhair SA, Erzurum SC. Oxidative and nitrosative events in
511 asthma. *Free Radic Biol Med* 2003; 35: 213-225.

512 43. Ben Anes A, Ben Nasr H, Fetoui H, Bchir S, Chahdoura H, Yacoub S, Garrouch A, Benzarti
513 M, Tabka Z, Chahed K. Alteration in systemic markers of oxidative and antioxidative
514 status in Tunisian patients with asthma: relationships with clinical severity and airflow
515 limitation. *J Asthma* 2016; 53: 227-237.
516 44. Sugiura H, Ichinose M. Oxidative and nitrative stress in bronchial asthma. *Antioxid Redox*
517 *Signal* 2008; 10: 785-797.
518 45. Toblli JE, Cao G, Giani JF, Dominici FP, Angerosa M. Markers of oxidative/nitrosative
519 stress and inflammation in lung tissue of rats exposed to different intravenous iron
520 compounds. *Drug Des Devel Ther* 2017; 11: 2251-2263.
521 46. Friedmann Angeli JP, Schneider M, Proneth B, Tyurina YY, Tyurin VA, Hammond VJ,
522 Herbach N, Aichler M, Walch A, Eggenhofer E, Basavarajappa D, Radmark O,
523 Kobayashi S, Seibt T, Beck H, Neff F, Esposito I, Wanke R, Forster H, Yefremova O,
524 Heinrichmeyer M, Bornkamm GW, Geissler EK, Thomas SB, Stockwell BR,
525 O'Donnell VB, Kagan VE, Schick JA, Conrad M. Inactivation of the ferroptosis
526 regulator Gpx4 triggers acute renal failure in mice. *Nat Cell Biol* 2014; 16: 1180-1191.
527 47. Linkermann A, Skouta R, Himmerkus N, Mulay SR, Dewitz C, De Zen F, Prokai A,
528 Zuchtriegel G, Krombach F, Welz PS, Weinlich R, Vanden Berghe T, Vandenabeele
529 P, Pasparakis M, Bleich M, Weinberg JM, Reichel CA, Brasen JH, Kunzendorf U,
530 Anders HJ, Stockwell BR, Green DR, Krautwald S. Synchronized renal tubular cell
531 death involves ferroptosis. *Proc Natl Acad Sci U S A* 2014; 111: 16836-16841.
532 48. Martin-Sanchez D, Ruiz-Andres O, Poveda J, Carrasco S, Cannata-Ortiz P, Sanchez-Nino
533 MD, Ruiz Ortega M, Egido J, Linkermann A, Ortiz A, Sanz AB. Ferroptosis, but Not
534 Necroptosis, Is Important in Nephrotoxic Folic Acid-Induced AKI. *J Am Soc Nephrol*
535 2017; 28: 218-229.

536 49. Wang H, An P, Xie E, Wu Q, Fang X, Gao H, Zhang Z, Li Y, Wang X, Zhang J, Li G,
537 Yang L, Liu W, Min J, Wang F. Characterization of ferroptosis in murine models of
538 hemochromatosis. *Hepatology* 2017; 66: 449-465.
539 50. Alvarez SW, Sviderskiy VO, Terzi EM, Papagiannakopoulos T, Moreira AL, Adams S,
540 Sabatini DM, Birsoy K, Possemato R. NFS1 undergoes positive selection in lung
541 tumours and protects cells from ferroptosis. *Nature* 2017; 551: 639-643.
542 51. Liu B, Zhao C, Li H, Chen X, Ding Y, Xu S. Puerarin protects against heart failure induced
543 by pressure overload through mitigation of ferroptosis. *Biochem Biophys Res Commun*
544 2018; 497: 233-240.
545 52. Wenzel SE, Tyurina YY, Zhao J, St Croix CM, Dar HH, Mao G, Tyurin VA,
546 Anthonymuthu TS, Kapralov AA, Amoscato AA, Mikulska-Ruminska K, Shrivastava
547 IH, Kenny EM, Yang Q, Rosenbaum JC, Sparvero LJ, Emlet DR, Wen X, Minami Y,
548 Qu F, Watkins SC, Holman TR, VanDemark AP, Kellum JA, Bahar I, Bayir H, Kagan
549 VE. PEBP1 Wardens Ferroptosis by Enabling Lipoxygenase Generation of Lipid Death
550 Signals. *Cell* 2017; 171: 628-641 e626.
551 53. Zosky GR, Iosifidis T, Perks K, Ditcham WG, Devadason SG, Siah WS, Devine B, Maley
552 F, Cook A. The concentration of iron in real-world geogenic PM(1)(0) is associated
553 with increased inflammation and deficits in lung function in mice. *PLoS One* 2014; 9:
554 e90609.

555

556

557

558

559

560

Supplementary figure legends

Figure E1. Iron diets and HDM-induced experimental asthma protocol.

Figure E2. House dust mite (HDM)-induced experimental asthma. Six-8-week-old wild-type (WT) BALB/c mice were intranasally administered HDM antigen for 5 days per week for 6 weeks and then major features of experimental asthma were assessed. Total and differential immune cells were enumerated in bronchoalveolar lavage and cytospin slides stained with May-Grunwald-Giemsa (A). Tissue eosinophil numbers were assessed in chrome salt fixation-stained lung sections (B). Mucus secreting cells (MSCs) were enumerated around inflamed airways in PAS-stained lung sections (C, D). Area of collagen deposition surrounding the basement membrane of small airways was quantified in Sirius red-stained lung tissue sections, in 6-8 airways/mouse, using *ImageJ* (E). Airway hyper-responsiveness (AHR) was measured in terms of central airway resistance (Rn) to inhaled increasing concentrations of nebulised methacholine (Mch) using Flexivent apparatus (F). Scale bar: 50 μm. Data are presented as mean ± SEM (n=6-8), pooled from two repeat experiments. **p<0.01; ***p<0.001; ****p<0.0001 compared to PBS controls.

Figure E3. Bronchoalveolar lavage (BAL) cell profiles in house dust mite (HDM)-induced experimental asthma in WT and *Hfe*$^{-/-}$ AKR mice. HDM was administered to ~36 week-old wild-type (WT) and *Hfe*$^{-/-}$ AKR mice for 5 days per week for 6 weeks and then differential immune cells were enumerated in BAL and cytospin slides stained with May-Grunwald-Giemsa. Data are presented as mean ± SEM (n=6-10), pooled from 2 repeat experiments. *p<0.05; **p<0.01; ***p<0.001.

Supplementary tables

585 **Table E1.** Custom-designed primers for human mRNA used in qPCR analyses.

586 **Table E2.** Custom-designed primers for mouse mRNA used in qPCR analyses.

587 **Table E3.** Antibodies used for flow cytometry

588 **Table E4.** Antigenic definitions for macrophage analyses conducted by flow cytometry

589 **Table E5.** Human bronchial airway epithelial cells (pBECs) donor characteristics

590 **Table E6.** Human airway smooth muscle cell and lung fibroblast donor characteristics

591

592 **Figure E1.**

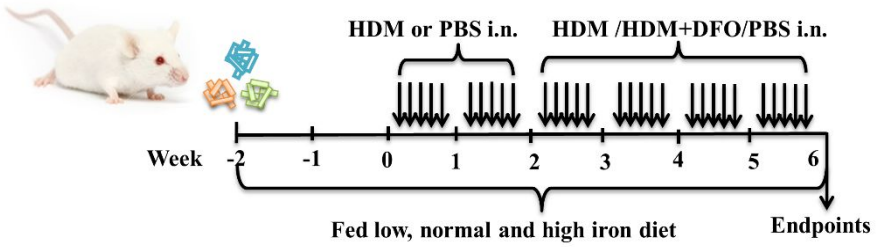

593

594

595

596

597

598

599

600

601

602

Figure E2.

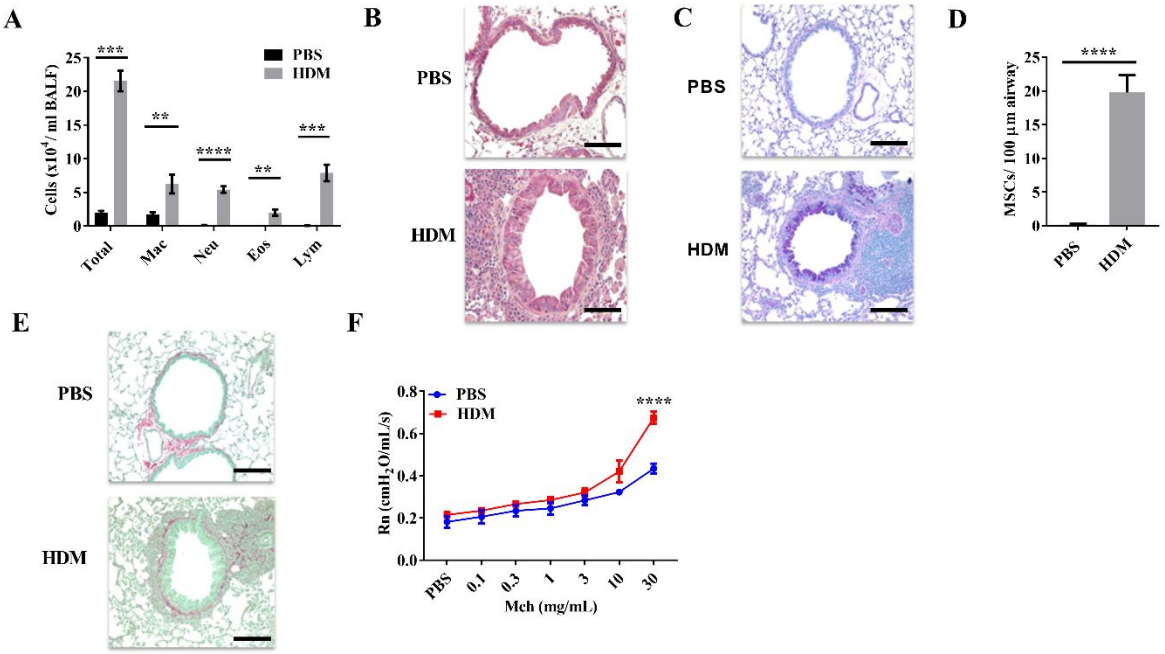

Figure E3.

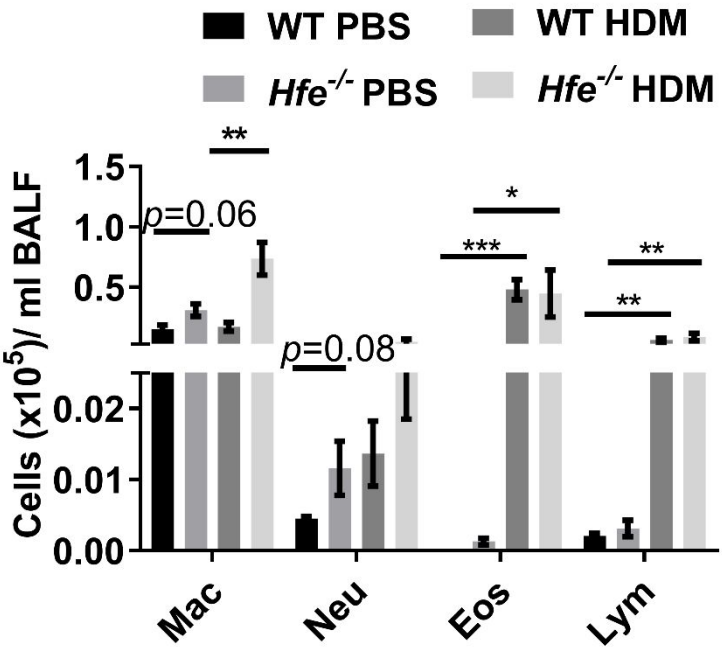

Table E1.

Primer	Primer sequence (5' → 3')	Target gene
Beta Actin Forward	CTGGCACCACACCTTCTA	*Beta Actin*
Beta Actin Reverse	GGTGGTGAAGCTGTAGCC	*Beta Actin*
DMT1 Forward	GGT GTT GTG CTG GGA TGT TA	*DMT1*
DMT1 Reverse	AGTACATATTGATGGAACAG	*DMT1*
FPN Forward	CTGTGCCCATAATCTCTGTC	*FPN*
FPN Reverse	CCATTTATAATGCCTCTTTCAG	*FPN*
HAMP Forward	CTGTTTTCCCACAACAGACG	*HEPC1*
HAMP Reverse	CAGCACATCCCACACTTTGA	*HEPC1*
TFR1 Forward	AGGAACCGAGTCTCCAGTGA	*TFR1*
TFR1 Reverse	ATCAACTATGATCACCGAGT	*TFR1*
TFR2 Forward	GGAGTGGCTAGAAGGCTACCTCA	*TFR2*
TFR2 Reverse	GGTCTTGGCATGAAACTTGTCA	*TFR2*
FTL Forward	CCATGAGCTCCCAGATTCGT	*Ft L*
FTL Reverse	TTCCAGAGCCACATCATCGC	*Ft L*
FTH Forward	CCAGAACTACCACCAGGACT	*Ft H*
FTH Reverse	CACATCATCGCGGTCAAAGT	*Ft H*
ZIP14 Forward	GCTTATGGAGAACCACCCCT	*ZIP14*
ZIP14 Reverse	AGGTTCCTGTGTCCTTGCAC	*ZIP14*
NRAMP1 Forward	TTCTCGTCCAAAGGAGCAGG	*NRAMP1*
NRAMP1 Reverse	GTTGCAGGCGGAACAGAAAG	*NRAMP1*
IRP1 Forward	CGTGCAGTCGGAGGAACAC	*IRP1*
IRP1 Reverse	TCGAAAATGGTAAGCGCCCA	*IRP1*

Table E2.

Primer	Primer sequence (5' → 3')	Target gene
Hprt Forward	AGGCCAGACTTTGTTGGATTTGAA	*Hprt*
Hprt Reverse	CAACTTGCGCTCATCTTAGGCTTT	*Hprt*
Il13 Forward	TGCTTGCCTTGGTGGTCT	*Il13*
Il13 Reverse	GGGGAGTCTGGTCTTGTGTG	*Il13*
Tfr1 Forward	CCCATGACGTTGAATTGAACCT	*Tfr1*
Tfr1 Reverse	GTAGTCTCCACGAGCGGAATA	*Tfr1*
***Il10* Forward**	AGGCGCTGTCATCGATTTCT	*Il10*
***Il10* Reverse**	ATGGCCTTGTAGACACCTTGG	*Il10*
***Ifng* Forward**	CTGGAGGAACTGGCAAAAGG	*Ifng*
***Ifng* Reverse**	TTGCTGATGGCCTGATTGTC	*Ifng*
***Tgfb1*Forward**	CCCGAAGCGGACTACTATGCTA	*Tgfb1*
***Tgfb1*Reverse**	GGTAACGCCAGGAATTGTTGCTAT	*Tgfb1*

Table E3. Antibodies used for flow cytometric staining

Antigen	Fluorophore	Clone	Manufacturer
CD45	PerCP	30F-11	Biolegend
CD11c	Brilliant violet (BV)421	N418	Biolegend
CD11b	Alexa Fluor (AF)700	M1/70	BD Biosciences
SiglecF	Phycoerythrin (PE)	E50-2440	BD Biosciences
F4/80	BV711	T45-2342	Biolegend
Ly6C	PE-Cy7	A1-21	BD Biosciences
TFR1	APC	R17217	Biolegend

Table E4. Antigen definitions for macrophage flow cytometric staining

Granulocyte type	Antigen definition
Total macrophages	$CD45^{+}$, $F480^{+}$, $CD11c^{hi/+/-}$, $SiglecF^{-/hi}$
Alveolar Macrophage	$CD45^{+}$, $F4/80^{+}$, $CD11b^{-}$, $CD11c^{hi}$ $SiglecF^{hi}$
Interstitial Macrophage	$CD45^{+}$, $F4/80^{+}$, $CD11b^{+}$, $CD11c^{+}$, $SiglecF^{-}$, $Ly6C^{-}$
Monocytes	$CD45^{+}$, $F4/80^{+}$, $CD11b^{+}$, $CD11c^{-}$, $SiglecF^{-}$, $Ly6C^{+}$

Table E5.

Characteristic	Healthy	Asthmatics
Number of subjects, n	8	7
Age, yr	62.63 ± 5.873	56.86 ± 5.595
Sex, M/F	2/6	2/5
FEV1% predicted	84.25 ± 5.230	78.43 ± 6.931
FEV1/FVC	0.747 ± 0.030	0.723 ± 0.021
ACQ	-	2.400 ± 0.623
Total cells ($x10^6$/mL BAL)	0.667 ± 0.391	3.717 ± 3.345
Macrophages (%)	47.75 ± 13.93	41.67 ± 13.48
Neutrophils (%)	22.75 ± 11.00	44.29 ± 14.64
Eosinophils (%)	0.850 ± 0.217	1.833 ± 0.363
ICS, yes/no	NA	7/0
ICS dose$	NA	717.10 ± 114.7
LABA, yes/no	NA	6/1
LAMA, yes/no	NA	2/5
SABA, yes/no	NA	3/4
OCS, yes/no	NA	0/7

M/F, male/female; FEV1, forced expiratory volume in one second; FVC, forced vital capacity; ACQ, asthma control questionnaire; BAL, bronchoalveolar lavage; NA, not applicable; ICS, inhaled corticosteroids; LABA, long-acting β2-agonist; LAMA, long-acting muscarinic antagonist; SABA, short-acting β-agonist; OCS, oral corticosteroids; yr, year. $Equivalent to Fluticasone µg/day. Data are shown as mean ± SEM.

Table E6.

Patient No.	Disease	Gender	Age
1	Pulmonary fibrosis	F	54
2	Pulmonary fibrosis	M	64
3	Bronchiectasis	M	60
4	IPF	M	65
5	Telomere-associated pulmonary fibrosis	F	45
6	COPD	M	61
7	NSCC	F	60
8	Pulmonary fibrosis	M	68
9	Emphysema	F	57
10	Emphysema	M	65
11	bronchiectasis	F	38
12	BOS (re-do)	F	28

13	Emphysema	M	60
14	Pulmonary fibrosis	M	53

631 M, male; F, female.

632